Quantification of water stress induced within-field variability of carbon dioxide fluxes in a sugar beet stand

M. Herbst[1], **P. Pohlig**[1], **A. Graf**[1], **L. Weihermüller**[1], **M. Schmidt**[1], **J. Vanderborght**[1], **H. Vereecken**[1]

[1] Agrosphere Institute, IBG-3, Forschungszentrum Jülich GmbH, Germany

Correspondence to: M. Herbst (m.herbst@fz-juelich.de)

Abstract

Net ecosystem exchange of carbon dioxide (NEE) and soil respiration at field scale can exhibit considerable spatial variability linked to the heterogeneity of soil properties and state variables. In this study, we measured NEE with the eddy covariance (EC) method in a sugar beet field characterized by high spatial variability in soil physical properties. We further measured NEE and soil respiration by chambers as well as soil water content and temperature at 18 locations within the field.

Spatially averaged chamber-measured NEE showed good agreement to the EC-based data. During a dry period high spatial variation of within-field NEE was detected with the chamber method. The coefficient of variation was on average 0.57 during the dry period, with a maximum of 0.72. Based on the depth-specific soil water content measurements the AgroC ecosystem model was inverted for soil hydraulic properties at each of the 18 locations, where soil water content was measured. Analyzing the model results revealed that root water uptake stress was the main driver of spatial and temporal variability in crop development and NEE, whereby the soil coarse material fraction (gravel content) and thickness of the layer above a gravel dominated soil layer were identified as the main influencing soil properties.

The chamber-measured NEE and the flux footprint analysis showed that particularly during periods of severe root water uptake stress EC-based measurements would be prone to biases. A combination of the footprint model with the AgroC ecosystem model estimated a bias of 14 % for the dry period and a vegetation period bias of 6 % in relation to the average CO_2 flux.

Keywords: spatial variation; net ecosystem exchange; respiration; eddy covariance; crop model; water stress

1. Introduction

Agricultural ecosystems are characterized by a high potential for carbon sequestration since their soils are managed intensely (Minasny et al., 2017). The estimation of net biome productivity for agricultural ecosystems is based on a balance of net ecosystem exchange of carbon dioxide (NEE), carbon exports, such as the harvested biomass and carbon imports, such as organic amendments. NEE represents a highly relevant term in the carbon balance, and precise quantification of NEE is required (Davis et al., 2010). At field scale, the eddy covariance (EC) method is commonly applied to estimate a spatially integrated NEE (e.g. Baldocchi, 2014; Post et al., 2015). However, carbon dioxide fluxes at field scale can exhibit considerable spatial variability linked to the heterogeneity of soil properties and state variables (Kutsch et al., 2005; Kupisch et al., 2015). The EC method measures the carbon dioxide fluxes within a footprint. Since this footprint varies temporally and spatially with wind sectors, spatial variation in NEE is difficult to measure with the EC method. If certain wind directions prevail and the carbon dioxide fluxes within this footprint are not representative for the entire field, then the EC-based estimates of NEE may be biased (Post et al., 2015). The potential level of this bias is related to the plot-scale spatial variability in carbon dioxide fluxes and the spatial scale of these variations with respect to the scale of the EC footprint. Thus, an assessment of this spatial heterogeneity is required to put appropriate and reliable limits on NEE estimates (Riutta et al., 2007; Petrone et al., 2008; Davis et al., 2010).

Studies on the quantification of the spatial variability of NEE within an otherwise homogeneous land use unit under agricultural practice are rare. A number of studies is related to the field scale spatial variability of soil CO_2 fluxes such as e.g. Herbst et al. (2012) or Prolingheuer et al. (2014). Further, studies characterizing the spatial variability of crop yield, which could be interpreted as a proxy for the spatial variability in seasonal cumulative gross primary productivity, as linked to the heterogeneity in soil properties do exist (e.g. Joernsgaard and

Halmoe, 2003; Hakojärvi et al., 2013; Stadler et al., 2015). The spatial variation in plant community within the EC flux footprint of a boreal fen was used in an upscaling procedure applied to point-scale chamber-based NEE measurements and the comparison with the EC estimates revealed good agreement (Riutta et al., 2007). Petrone et al. (2008) also performed chamber-based NEE measurements to determine the spatial variability of NEE within open and riparian grasslands. They conclude, that much of the spatial variation in NEE could be explained by variations in aboveground biomass and canopy height as a consequence of soil nutrient status. Davis et al. (2010) applied a two-tower EC approach to determine the variation in NEE in a spring barley stand and found that within-plot spatial variation was mostly larger than the effect of conventional tillage vs. no-tillage management. The authors stressed the need to address the uncertainty in NEE measurements in agricultural settings resulting from spatial variations within the EC flux footprint. Kupisch et al. (2015) performed repeated measurements of NEE using eight chambers within a field cropped with winter wheat and winter barley. They detected significant spatial variations in NEE, mainly related to the patterns of leaf area index resulting from the underlying pattern of water supply.

In relation to other crops, sugar beet is known to react rather sensitively to root water uptake limitations (Brown and Biscoe, 1985; Tognetti et al., 2003, Fitters et al., 2018). Rudolph et al. (2015) detected distinct patterns of water stress within a sugar beet stand resulting from a paleo-channel river system in test field F01 near Selhausen, Germany. In this setting, subsoil heterogeneity obviously generated a pattern in water stress, that was even discernible by eye. Unfortunately, root water uptake stress is rather difficult to measure directly and it is even more difficult to upscale water stress from single plants to representative areas. Models, on the other hand, offer the opportunity to estimate water stress, given that valid information on evapotranspiration demand and soil water status is available (Cai et al., 2017). In this study we combine the agroecosystem model AgroC (Herbst et al., 2008; Klosterhalfen et al., 2017) with

the eddy covariance flux footprint model of Kormann and Meixner (2001). Commonly applied agroecosystem or agronomic models like AquaCrop (Raes et al., 2017) or WOFOST (Boogard et al., 2014) also account for the effect of the soil water status and root water uptake stress on photosynthetic activity, which subsequently affect crop growth dynamics and allometry. Such models are thus highly suitable to estimate spatio-temporal variations in NEE.

In this study, we combine chamber and EC-based NEE measurements, point-scale measurements of soil respiration, soil temperature, soil water content and crop physiology with agroecosystem modelling in order to assess and to understand the pattern of within-field scale carbon dioxide fluxes. The specific goals of this study were: (i) to quantify the within-field spatial variation in NEE and soil respiration using chamber measurements, (ii) to compare eddy covariance-based integral estimates of NEE to the chamber measurements, (iii) to identify and reproduce the mechanism generating the spatial pattern in NEE with a physically-based agroecosystem model, and (iv) to quantify the potential bias in EC data resulting from the spatial variation in NEE.

2. Material and Methods

For the vegetation period 2016 we selected 18 locations (p1 to p18) within a sugar beet (*Beta vulgaris L.*) stand, at which soil water content and soil temperature were recorded with hourly resolution. Chamber-based measurements of NEE and soil respiration were performed on a weekly basis. Basic soil properties were available at these sites. At two of the 18 locations measurements were intensified in terms of soil respiration and biometric features. At both locations, p2 and p16 (see Fig. 1), located either within or outside a paleo-channel, soil respiration was measured with up to 5 chambers in parallel at hourly resolution. Further, leaf area index, aboveground and sugar beet dry mass was determined five times over the vegetation period at the two locations.

2.1 Experimental site

The centre of the 2.8 ha field site 'F01' is located near Selhausen, Germany at 50° 52' 0.09''N 6° 27' 21.5''E, 112 m a.s.l. The field is embedded in the Lower Rhine Embayment and characterised by a mean precipitation of 715 mm y^{-1} and a mean air temperature of 10.2°C (Rudolph eat al., 2015). The field is cultivated with the typical regional crop rotation of winter cereals and sugar beet. Pesticide application in 2016 was performed according to regional standard practice. Mineral fertilizer was applied on April 3 (950 kg NPK ha^{-1}) and on July 15 Epsom salt was applied at 5 kg ha^{-1}. Soils are classified as cambisols (IUSS Working Group WRB, 2007), composed of upper terrace Pleistocene sands and gravels, which are covered by aeolian sediments (loess) of variable thickness. Rudolph et al. (2015) detected a paleo river system within the field, which creates a large spatial variability. Shallow soils developed in rather coarse textured materials can be found close to deep soils composed of fine textured sediments. A cluster analysis based on electromagnetic induction (EMI) data using various coil configurations with two target clusters allowed for an identification of sampling sites within or outside the loamy paleo-channel materials. Notably, the selection of the sampling locations was based on the EMI data gathered at the site in 2015 using the same approach as described in detail by Brogi et al. (2019). According to the cluster algorithm the sampling locations p1, p2, p4, p6, p10, p11, p12, p15 and p18 were within the paleo-channel, whereas locations p3, p5, p7, p8, p9, p13, p14, p16 and p17 were outside the channels in the rather coarse textured materials. The soil sampling and profile layering observed during the installation of the soil water content sensors basically confirmed the EMI-based clustering.

2.2 Measurements

2.2.1 CO_2 fluxes

Point-scale NEE flux measurements were performed with a portable closed plexiglass chamber, covering a ground surface of 1 m^2. The lower part of the setup consisted of a permanently installed aluminium frame inserted ~5 cm into the soil. The upper part of the chamber was available at different sizes, which allowed to adapt chamber volume to crop height. Four air mixing fans were installed in the chamber corners and CO_2 concentration change over time was monitored with an infrared gas analyser LI8100 (Licor Biosciences, Lincoln, NE, USA). The NEE chamber design was identical to the one described by Langensiepen et al. (2012). NEE chamber closure time was 120 s with a lag-time of 5 s. At each sampling campaign the 18 locations were sampled between 11:00 and 13:00 CET. For each weekly sampling the average over the 18 sampling locations was calculated. For correlations with EC data, the sampling campaign average was related to the corresponding 12:00 CET EC-measured flux.

Soil respiration measurements were performed with an automated non-steady-state closed chamber system (LICOR 8100-103, Licor Biosciences, Lincoln, NE, USA). PVC collars with 20 cm diameter and a height of 7 cm were installed into the soil such that ~2 cm of the collar protruded above the soil level. Respiration chamber closure time was 120 s and the linear concentration increase in CO_2 was used to calculate soil CO_2 efflux. The weekly field scale measurements at 18 locations were performed with the hand-held survey chamber during daytime, whereas the continuous measurements during both daytime and nighttime at p2 and p16 were performed with four to five automated chambers and the Li8100 multiplexer systems.

Due to practical issues with power supply during spring 2016 a large gap in the respiration data of p16 was filled with data estimated from the respiration measurements at p2. A linear regression was established between respiration fluxes of p2 and p16 for the first half of the measurement period, during which respiration at p2 and p16 was reasonably correlated (R^2=0.87), and was then used to calculate respiration flux at p16. Without such gap-filling, high fluxes during spring would not have been captured at p16, which subsequently would have caused biased estimates in the inversion approach for the modelling of soil respiration.

The eddy covariance (EC) tower was located near the centre of field F01 (see Fig. 1) and the EC devices were installed 2 m above ground. Raw data was collected at a 20 Hz frequency and flux processing was performed for half-hour intervals. For the entire EC processing the TK3.1 sofware (Bayreuth, Department of Micrometeorology, Germany; Mauder and Foken, 2011) was used, implementing the standardized method for EC data processing and quality assurance as proposed in detail by Mauder et al. (2013). For this study only flux measurements of the highest quality level were used and gap-filling was not performed. Hourly values of EC-based NEE were calculated by arithmetic averaging. To quantify the contribution from areas within and outside of the paleo-channels on the measured EC fluxes, and to exclude measurements that are affected by surrounding areas, the flux footprint model by Kormann and Meixner (2001) as implemented in TK3 (Mauder and Foken, 2011) was used. From measurement height, canopy height and measured micrometeorological parameters it computes source weights on a 2 x 2 m grid.

2.2.2 Other measurements

Leaf area index (LAI) and biomass were determined at five dates over the vegetation period by sampling 1 m rows in the vicinity of p2 and p16, keeping a distance of at least 2 rows to the collars. Green and brown leaves were separated before LAI was measured with a leaf area meter (LI-3100C, Licor Biosciences, Lincoln, NE, USA). Organ specific biomass was measured by determining the dry weight after oven-drying for 24 h at 105 °C.

Soil water content and soil temperature was measured in hourly resolution at three depths (10, 20 and 50 cm) at each of locations p1 to p18 using the wireless sensor network SoilNet (Bogena et al., 2010). A total of 108 sensors was installed after the sowing (April 10, 2016), with two replicate sensors installed at each depth.

In the course of the SoilNet installation undisturbed and disturbed soil samples were collected for the ploughed topsoil horizon Ap at a depth of 5-10 cm and for the uppermost subsoil horizon, further referred as the B horizon, at 40-45 cm depth. The disturbed sample material was analysed for soil organic carbon content, fine texture (< 2 mm) and coarse fraction (> 2 mm). The latter was determined gravimetrically by wet sieving of ~10 L sampling volume and volumetric stone fraction was calculated assuming the stone material had the density of quartz (2.65 g cm^{-3}). Gravimetric clay (< 2 μm), silt (2-63 μm) and sand (63-2000 μm) fractions were measured by the combined wet sieving and sedimentation method according to DIN ISO 11277 (2002). Gravimetric soil organic carbon contents were determined via dry combustion with an elemental analyser (Fisons NA 2000, USA). Drilling with a hand auger down to the gravel layer or to a maximum of 1.5 m was additionally performed to record the total profile depth and horizon thickness (Fig. S1, supplementary material).

2.3 Spatial variation and temporal persistence

We followed the approach suggested by Vachaud et al. (1985) by quantifying the temporal persistence with the Pearson correlation coefficient between two spatial patterns of fluxes determined at back-to-back measurement campaigns and with ranked mean relative differences (MRD). The latter provides an estimate of the mean deviation measured at a specific sampling location in relation to the overall spatial mean and was calculated according to:

$$MRD_i = \frac{1}{m}\sum_{j=1}^{m}\frac{a_{i,j}-a_{avg,j}}{a_{avg,j}} \quad (1)$$

where m is the number of measurement dates, $a_{i,j}$ represents the variable value at sampling location i and time j and $a_{avg,j}$ represents the mean of all sampling location values at the same time.

2.4 Agroecosystem model setup

2.4.1 Model description and input variables

AgroC is based on three sub-modules. SoilCO2 (Simunek and Suarez, 1993) is a one-dimensional model for the flux of water, heat, and CO_2 in soils. The heterotrophic production of CO_2, i.e. the turnover of soil organic carbon, is simulated with the RothC pool concept (Coleman and Jenkinson, 2005), whereas the crop growth module SUCROS (Spitters et al., 1989) accounts for the autotrophic part of soil respiration, carbon dioxide assimilation by photosynthesis and all other crop related processes. A more detailed description of the coupling can be found in Herbst et al. (2008) and in the appendices of Klosterhalfen et al. (2017) and Brogi et al. (2020). For this study, the most relevant part of the coupling refers to the effect of

root water uptake stress on carbon dioxide assimilation. The potential sink term of root water uptake is estimated from the relative root density profile over depth and potential transpiration, calculated according to the FAO method (Allen et al., 1998) and split into evaporation and transpiration according to Beer's law in dependence of the LAI. The actual root water uptake is estimated in dependence of the simulated soil pressure head profile following the commonly applied approach of Feddes et al. (1978):

$$\alpha(h) = \begin{cases} \frac{h_0 - h}{h_0 - h_1} & h_0 \leq h \leq h_1 \\ 1 & \text{for} \quad h_1 \leq h \leq h_2 \\ 10^{\frac{h_2 - h}{h_3}} & h_2 \leq h \leq h_3 \end{cases} \tag{2}$$

With dimensionless water stress indicator α (between 0 and 1), four pressure head threshold values h_0 to h_3, and soil pressure head h. The scaling of the potential root water sink term with α gives the actual root water sink term at a specific rooting depth. The integral of the actual root water uptake over the profile equals actual transpiration. Subsequently, the ratio of actual to potential transpiration is used to scale the potential (non-stressed) carbon dioxide assimilation rate. We further refer to the averaged, root density weighted α over the profile as the average water stress indicator α_{avg}.

The measured depth to the gravel layer was used as the total simulation profile depth. The spatial discretisation was 1 cm for the lower part of the profile and was decreased to 0.5 and 0.1 cm near soil surface. The lower boundary condition was free drainage and atmospheric water fluxes in terms of precipitation and potential evaporation were used as upper boundary

condition. The maximum rooting depth was restricted to the total profile depth, assuming that the sugar beet roots did not penetrate into the gravel layers (Fitters et al., 2018), which was confirmed in the field when the SoilNet sensors were removed. The root density profile over soil depth is given in Table S6 in the supplementary material.

For soil temperature, the thermal soil properties were estimated according to Chung and Horton (1987) and the upper boundary condition was provided by the soil temperatures measured near the EC station at the soil surface. The lower boundary condition was a fixed temperature, assuming a long-term average of 8°C.

The heterotrophic production of soil CO_2 was calculated from the decomposition of the carbon pools, which were estimated assuming turnover equilibrium according to Weihermüller at al. (2013) from the depth-specific measured soil organic carbon contents. The soil temperature dependency of soil carbon decomposition was simulated with an Arrhenius-type equation (Simunek and Suarez, 1993) assuming a reference temperature of 8°C. The soil water content dependency of soil carbon decomposition was prescribed also following the approach of Simunek and Suarez (1993).

2.4.2 Inversion and validation

All model inversions were performed with the Shuffled Complex Evolution (SCE-UA) algorithm developed by Duan et al. (1992), which is classified as a global optimization routine. The sum of the squared errors defined the objective function value.

In a first step, some default crop parameters were adjusted manually to match observations in terms of leaf area index (LAI) and organ-specific crop biomasses. The Feddes threshold

parameter h_2 was set to -4000 cm, whereas the default maximum photosynthetic rate at light saturation of 45 kg CO_2 ha^{-1} leaf h^{-1} was used. For p16 the assimilate fraction allocated to the shoot for effective temperature sums of 400, 900 and 901°C were set to 0.38, 0.28 and 0.12, whereas the default values of 0.43, 0.55 and 0.17 were kept for the p2 model. This was done to account for a feedback between water stress and crop physiology. The underlying assumption is that a crop with persistent water stress invests more biomass in the root system. This root/shoot partitioning is the only difference in the crop parameters for the p2 and p16 model. A list of the main crop parameters can be found in the supplementary material in Table S5.

The soil hydraulic properties in terms of the Mualem/van Genuchten (MvG) parameters for the A_p and the B horizon of locations p1 to p18 were determined in the lab with the Hyprop apparatus (Meter Group, Munich, Germany). The first model runs revealed that the lab determined MvG parameters did not provide a good match between measured and simulated soil water contents. Therefore, the inverse of the air entry pressure α, the slope parameter *n* and saturated hydraulic conductivity K_s were inversely estimated. Water content at saturation θ_s was fixed as given from the Hyprop measurements at saturation. During the fitting of the MvG parameters using the Hyprop measurements the residual water content θ_r was set to zero since this provided optimum match. However, this did not provide adequate fits to the field measured water contents. Using the pedotransfer functions of Rawls and Brakensiek (1985) and Brakensiek and Rawls (1994) allowed to estimate θ_r from fine texture, coarse fraction (> 2 mm), and bulk density and subsequently provided good fit to the field-measured water contents. Finally, θ_r and θ_s were fixed in the inversion procedure using field measured water contents to keep the number of inversely estimated hydraulic properties at minimum.

After the inversion for the soil hydraulic properties, the measured soil CO_2 fluxes were used to invert the parameters h_{b1} and h_{b2} that define the reduction of carbon decomposition in dependence of pressure head according to Simunek and Suarez (1993). The parameters were estimated for p2 and p16 separately, since water contents, textural composition and estimated root respiration differed for the two locations.

Based on the models established for p2 and p16, we set up models for the 16 other locations equipped with SoilNet sensors. The soil water contents measured at each of the locations were again used to inversely estimate soil hydraulic parameters, analogue to the intensely monitored sites p2 and p16. The estimated soil hydraulic parameters are summarized in Table S3 of the supplementary material. The soil respiration parameters and the root/shoot partitioning parameters, as assumed for p2 and p16, were assigned to the other sites according to their cluster membership. Sites p1, p2, p4, p6, p10, p11, p12, p15, and p18 were run with the p2 parameterizations (within the paleo-channel), whereas sites p3, p5, p7, p8, p9, p13, p14, and p17 were run with the p16 parameterization for soil respiration and root/shoot partitioning (outside the paleo-channel). Apart from the soil hydraulic parameters and the soil heterotrophic respiration parameters, the model parameters within a cluster group were thus identical. We further refer to models p1 to p18 as the 'model ensemble', and to the ensemble of models within the paleo channel as the 'loamy' cluster and to the ensemble of models outside the paleo-channel as the 'stony' cluster.

Four criteria were applied to quantify the agreement between model and measurement. The mean absolute error MAE and the root mean square error RMSE provide error measures in the units of the selected variable. The coefficient of determination R^2 and the coefficient of model efficiency ME (Nash and Sutcliffe, 1970) are dimensionless. R^2 varies between 0 and 1, whereas the ME varies between $-\infty$ and 1. R^2 can reach high values close to 1 even if only the

pattern (but not the magnitude of values or their variance) is reproduced well by the model. In contrast, the ME is also sensitive to the agreement of the measured and simulated mean values, which points to a rather strict criterion. All validation criteria for sites p1 to p18 (except for sites p2 and p16) are summarized in Table S4 (supplementary material).

3. Results

3.1 *Chamber-based vs. eddy covariance NEE and soil respiration*

Comparing the mean of chamber-based NEE at the 18 sampling locations to the corresponding hourly value of the EC data reveals good agreement. Figure 2a shows that the temporal evolution of chamber-based and EC-measured NEE is similar, proven by a Pearson correlation coefficient of 0.76. The overall mean value of the chamber-based NEE during the experimental period, i.e. the mean of the 18 weekly sampling campaigns, is -542 mol CO_2 ha^{-1} h^{-1}. The corresponding EC value, i.e. the average of the 18 corresponding fluxes measured at noon by EC, is slightly lower with a value of -597 mol CO_2 ha^{-1} h^{-1}. A closer look to Fig. 2a reveals, that during the first part of the growing period, before Aug 19, chamber-based NEE nicely falls into the envelope of the EC-measured data. During the second period (after Aug 25), which is characterized by a much lower photosynthetic activity due to drought stress, the chamber-based NEE appears to be more negative in comparison to the EC data. Chamber-based averages for the first period and the dry period are -619 and -388 mol CO_2 ha^{-1} h^{-1}, respectively, whereas corresponding averages of EC measurements are -811 and -169 mol CO_2 ha^{-1} h^{-1}. A direct comparison of the soil respiration (R_s) measured with the soil chamber and night-time EC-measured NEE, which is often defined as ecosystem respiration, is not possible because the former is only available during day-time, while the latter is only available during night-time and also includes above-ground plant respiration. A visual inspection (Fig. 2a), however, shows good agreement in the overall magnitudes and timing of the positive fluxes.

3.2 *Spatial pattern and temporal persistence of carbon dioxide fluxes*

Figure 2a also shows the spatial variation of NEE and soil respiration, expressed as the standard deviations over the 18 sampling locations at a specific measurement date. According to this, the spatial variation of NEE is constantly higher than for soil respiration, which may be partly related to the fact that the absolute magnitude of NEE is higher than for soil respiration. The dimensionless coefficient of variation (CV) relates the standard variation to the mean and thus removes the effect of varying magnitudes. The CV of NEE varies between 0.13 (July 7) and 0.72 (Oct 20). Figure 2b shows, that the spatial variation in terms of CV is higher for NEE than for soil respiration, with the exception of three measurement dates, when the CV of NEE is slightly lower than for soil respiration. The CV of both, soil respiration and NEE, increases over time, proven by a slightly higher positive linear trend of $6.2*10^{-5}$ h^{-1} for the CV of NEE in relation to the positive linear trend of $2.8*10^{-5}$ h^{-1} determined for the CV of soil respiration. For NEE average CV before Aug 19 is 0.38. During the dry period following Aug 25 the average CV increases to a value of 0.57. The CV of soil respiration varies between 0.16 and 0.51 and also shows higher values during the dry period.

The computation of ranked MRDs allows for an identification of sites that behave over time similar to the spatial mean. In this respect, sampling locations p3 and p15 exhibit the lowest MRDs in terms of NEE (Fig. 3). The MRDs further allow for an identification of sites that exhibit values continuously higher (positive) or lower (negative) than the spatial mean. Locations p2, p4, p6, p7, p10, p11, p12 and p15 have positive MRDs and the top right map of Fig. 3 shows that, except for location p7, all these sites are clearly located with the paleo-channel system. The soil profile found at location p7 is special with respect to the thickness and the coarse fraction of the B horizon (see supplementary material Fig. S1). It is the only profile classified as outside the paleo-channels, which has a B horizon thickness of 120 cm in

combination with a rather low gravimetric coarse fraction of 12%. The locations p1 and p18, with MRDs of -0.21 and -0.15, were classified as being inside the paleo-channels but show negative MRDs. Both soil profiles, p1 and p18, are characterized by a low B horizon thicknesses of 50 and 20 cm, respectively, and by an A horizon coarse fractions of 18 and 14%. The remaining locations, p3, p5, p8, p9, p13, p14, p16 and p17 are members of the outside channel cluster and show negative MRDs for NEE. The most negative MRD of -0.47 was observed for p16, whereas the most positive MRD of NEE was recorded for p7 with a value of 0.36.

The pattern of MRDs for soil respiration follows to some extent the pattern observed for NEE, but not every site with a positive MRD for NEE also shows a positive MRD for soil respiration. Please note that for soil respiration a positive MRD indicates higher than average respiration activity, whereas a positive MRD of NEE indicates less photosynthetic activity, i.e. on average more positive NEE. Locations p2, p6, p7, p11, p12, p13, p15, and p18 are characterized by a positive MRD for soil respiration. Among those are the two sites p13 and p18 with a negative MRD for NEE, all other sites reveal positive MRDs for NEE. Except for locations p7 and p13 all locations with a positive MRD for soil respiration are sited within the paleo channels. Most of the sites with a negative MRD for soil respiration are located outside the paleo-channels, with the exception of sites p4 and p10. The most negative MRD for soil respiration with a value of -0.31 was recorded for p8, whereas the most positive one was captured for p7 with a value of 0.36.

The temporal persistence of NEE and soil respiration spatial patterns was quantified by computing the Pearson correlation between two consecutive measurement campaigns (see Table 1). The temporal correlation of the spatial patterns of NEE was rather low in the period before Aug 16, with correlation coefficients varying between 0.01 and 0.51. After Aug 19 higher correlation coefficients, varying between 0.21 and 0.92, were observed. According to

Fig. 2a drought occurs for the first time from Aug 25 onward. In relation to NEE the correlation of soil respiration patterns over time is more stable. It is at a medium level, with extremes of 0.05 and 0.86, and potentially also shows higher temporal stability over the last part of the growing period characterized by low soil water contents. This feature is not as pronounced as detected for NEE and only 6 measurement campaigns were performed for soil respiration over the period starting at Aug 19.

The analysis of MRDs revealed that the sites located within the paleo-channel, further referred to as the 'loamy' subset, expose on average systematically different NEE in relation to the sites located outside the paleo-channels (subset 'stony'). For Fig. 4 we split all chamber-based flux data into the loamy and the stony subset and computed mean and standard deviation. Before Aug 19 both subsets are basically in agreement regarding the mean and variation of NEE. Starting with the Aug 25 measurements, the NEE means of the subsets diverge and spatial variation increases. The loamy sites clearly show a more negative NEE than the stony sites until harvest. It is important to notice that the chamber-based fluxes shown in Fig. 4 for the loamy area represent the average fluxes measured at the 9 sampling locations and that the loamy cluster covers just 32 % of the test site area. Notably, even the chamber-based NEE of the stony subset slightly exceeds (i.e. is more negative) the fluxes measured by the EC method.

3.3 *Models at the intensively monitored sites*

We used the agroecosystem model to translate the temporally variable soil water status into root water uptake stress and the resulting effect on photosynthetic activity and crop development. First, AgroC model runs were established for sites p2 and p16, which had intensified monitoring and were expected to represent extremes in terms of root water uptake stress. Location p2 is characterized as an almost stone-free loamy soil with a B horizon up to a depth of at least 1.5 m (see Fig. S1 in the supplementary material). In contrast, p16 is a shallow

soil, practically without a B horizon, where the gravel layer was found directly below the Ap horizon at a depth of ~0.3 m. Further, at p16 the gravimetric coarse fraction in the Ap horizon was 21%. In the gravel layer the gravimetric coarse fraction was 75%.

The variation in soil profiles is clearly reflected in the soil water contents measured at the two locations. Figure 5 shows that the soil water content at p2 in a depth of 50 cm is at minimum with ~0.2 cm^3 cm^{-3} near the end of October, whereas the soil water content of p16 at 50 depth is near the residual water content of ~0.04 cm^3 cm^{-3} from July on. Water content in the upper part of profile p2 also drops from about 0.3 at mid of June to values below 0.1 cm^3 cm^{-3} near the end of July and remains well below 0.1 cm^3 cm^{-3} for most of the growing period. At location p2 water contents also decrease, but the drop in water content due to root water uptake is less pronounced and the depth-specific minimum water contents are always higher in relation to p16.

We used the measured soil water content at 10, 20, and 50 cm to inversely estimate the soil hydraulic parameters α, n and K_s for each horizon and location. During the inversion procedure we split the Ap horizon into two layers (Bauer et al., 2012) of 0.15 m thickness each. This modification drastically improved the model performance since the splitted Ap horizon better reflects the difference in soil structure of the upper part of the Ap horizon that is affected by soil management during seedbed preparation. According to Fig. 5, the model is in good agreement to the measurements and it is able to reproduce all the relevant features and differences between p2 and p16 in terms of measured water contents mentioned above. This is proven by all validation criteria and the model efficiency ME varying between 0.78 and 0.91 and between 0.87 and 0.92 at p2 and p16, respectively (see Table 2). The biggest discrepancy between model and measurement was observed for the soil water content of p2 at 10 cm depth, for which the drop in water content occurred a little too early; also, a rewetting not present in the measurements was estimated in September. At p2 also the water content at 20 and 50 cm

depth was estimated too low at the very beginning of the measurement period, which is mainly the result of improper initial conditions. The estimated soil hydraulic properties are summarized in Table S3 in the supplementary material.

Figure 5 also shows the differences in the simulated temporal evolution of the water stress factor α_{avg} defined as the profile average root water uptake stress according to Feddes et al. (1978). For site p2 very little water stress was estimated, whereas p16 is heavily stressed starting from August on. Severe water stress and even complete shut off of root water uptake was estimated for the beginning of September, when α_{avg} turns zero. Note, that the hourly gross assimilation is scaled with this stress factor, also switching the estimated photosynthetic activity off for that period. Thereafter, estimated root water uptake stress is still high, varying roughly around 0.3 for the rest of the growing season at p16.

In a next step, we investigated how the estimated water stress would propagate into biomass accumulation and sugar beet yield. The upper panel of Fig. 6 shows that the sugar beet dry mass of 14.8 t ha^{-1} estimated for p2 at harvest is higher by a factor of 1.7 in relation to the respective value of 8.7 t ha^{-1} simulated for p16. For both sites the beet dry mass is similar until mid of July, for the model and the measurements. Thereafter, when root water uptake stress occurs for p16 dry matter accumulation in the beet diverges. At p16 the sugar beet crops almost stopped accumulating biomass around August 25, whereas at p2 beet biomass was still increasing but at a much lower rate than before. The ME for beet dry mass of p2 and p16 is 0.84 and 0.9, respectively. This points to a reasonably good simulation of yield development. Beet mass appears to be slightly overestimated for p2 and slightly underestimated for p16. However, both measurements, at p2 and p16, indicate the highest beet biomass for the measurement date prior to the last measurement, which is rather unexpected. This might be related to the sampling procedure, where only a limited amount of biomass could be sampled in the vicinity of p2 and p16 in order to minimize disturbance. The development of leaf biomass is also affected by water

stress, which was reflected by the model as indicated by MEs of 0.7 and 0.65 for leaf dry mass and 0.93 and 0.74 for green LAI (lower panel Fig. 6), for p2 and p16, respectively.

The continuously chamber-measured soil respiration differs not much between sites p2 and p16 (Fig. 7). The difference in organic carbon content in the Ap horizon of 1.04 % at p2 and 1.07 % at p16 is also minor. With MEs of 0.72 and 0.61, for p2 and p16, respectively, the model performs reasonably well in terms of the temporal evolution and the overall level of soil respiration. The biggest discrepancies between model and measurement were observed during the first half of July for p16. Both, the simulated soil temperature (see supplementary material Fig. S7 and Table 2) and soil water contents (lower panel Fig. 5) indicate good model agreement, also in this period. Thus, this must be either related to an underestimation of root respiration or an inadequate relation between heterotrophic respiration and soil water content. Estimated threshold parameters h_{b1} and h_{b2} for the reduction of heterotrophic respiration in dependence of pressure head were -124 and -1786 cm for p2 and -892 and -20015 cm for p16, respectively.

The effect of decreased soil water availability is also apparent in the EC-based measurements of NEE (Fig. 8). Near the end of August, photosynthetic activity of the sugar beet plants rapidly decreases (i.e. NEE is less negative) to a value of about -350 mol CO_2 ha^{-1} h^{-1} at daily maximum and never recovers to values of about -1000 mol CO_2 ha^{-1} h^{-1} at daily maximum measured prior to the dry period. Both models, set up for p2 and p16, are in good agreement to the EC measurements before end of August. During the dry period, NEE simulated for p16 agrees well to the EC data, with the exception that the initial drop in carbon assimilation at the beginning of September is overestimated (i.e. NEE is too positive) by the AgroC model. The NEE of this period, on the other hand, is well reproduced by the p2 model. However, thereafter NEE estimated by AgroC for p2 is more negative than indicated by the EC data. Both models, established for p2 and p16, of course differ inherently from the EC-based NEE because they

were set up for single locations, whereas the EC data represents a spatially averaged flux. Even though, both models basically agree well to the EC data as shown by MEs of 0.79 and 0.68 for p2 and p16, respectively. The average NEE computed on the basis of the 2368 timesteps of EC measurements was -206 mol CO_2 ha^{-1} h^{-1} for the EC data and was -286 and -140 mol CO_2 ha^{-1} h^{-1} for the models of p2 and p16, respectively.

3.4 *Modelling of spatio-temporal patterns*

Based on the AgroC models for p2 and p16, models for the other 16 sites equipped with SoilNet sensors were established. In terms of soil water content, all models are in good agreement at the three measurement depths, indicated by ME well above 0.8, with the exception of the soil water content measured at 10 cm depth at site p18, which has the lowest overall ME of 0.75. The simulation of soil temperature is also basically in good agreement to the measurements at all sites, however, for the measurement depth of 50 cm rather low MEs, even below 0.5 were observed. This measurement is the least relevant for the simulation of soil heterotrophic respiration, as the soil organic carbon contents in the B Horizon are consistently low (see Table S2, Supplementary material). At the two upper measurement depths of soil temperature the lowest ME observed was 0.64 at p5 and all other sites show an ME higher than 0.7. After checking the agreement between soil state variables water content and temperature, the estimated soil respiration was validated against the chamber-measured soil respiration at each sampling location. The temporal correlation coefficient over the 17 measurement dates varied between 0.42 (p6) and 0.82 (p13) and was on average 0.65 over all sites (Table 3). This points to reasonably good simulations of the temporal course of soil respiration at each sampling location. The total average fluxes of measured and simulated soil respiration, 92 and 82 mol CO_2 ha^{-1} h^{-1}, respectively, are also in good agreement. However, the spatial correlation coefficient of 0.16, computed from the temporally averaged fluxes at each location, clearly

shows that the spatial variation of soil respiration was not captured by the model runs. The temporal correlation over the 18 measurement dates of chamber-based NEE and AgroC varied between 0.34 (p18) and 0.85 (p13) and was on average 0.66 over all sites (Table 3). For NEE the temporal variation was reproduced by the models, but also the spatial variation, quantified as the correlation coefficient of 0.63 between simulated and chamber-measured average NEE at each sampling location, agreed well. The total average of chamber-measured and model ensemble NEE was -563 and -506 mol CO_2 ha^{-1} h^{-1}, respectively. For NEE we further investigated, whether the AgroC model ensemble was able to reproduce the within-field variance as measured by the chambers and shown as the blue shaded surface in Fig. 2. We extracted the respective model ensemble data of the measurement dates and generated a comparable plot (Fig. 9). This shows that the model-estimated standard deviation was clearly lower during the first half of the vegetation period. But after mid of August, when significant root water uptake stress occurred, the model ensemble represents the chamber-measured within-field variation in NEE well, with the ensemble estimated variation being on average just slightly smaller than the observations.

The chamber data can also be used to evaluate the model performance of the loamy and the sandy model ensemble. The correlation coefficient over time between NEE estimated for the loamy and the sandy model cluster and the correspondingly averaged chamber-measured NEE was 0.72 and 0.83, respectively. Also, the difference in the observation period average of chamber measured NEE between the loamy and sandy area of 99 mol CO_2 ha^{-1} h^{-1} was quite well reproduced by the AgroC model difference of 125 mol CO_2 ha^{-1} h^{-1}.

3.5 Combination of footprint model and AgroC

The average fraction of the NEE flux footprint located within test site F01 over the observation period was 72 %, linked with a standard deviation of 17 %. Limiting the analysis to negative

NEE, i.e. the assimilation dominated daytimes, revealed a higher average footprint fraction of 78 % with a standard deviation of 12 %. We further analyzed for every hourly time step how large the sum of the footprint weights within the areas of the loamy (within paleo-channel) cluster and the stony (outside the paleo-channels) cluster was. The observation period average value for the stony cluster was 80% with a standard deviation of 17 %. The respective value of the loamy cluster was 20 % with a standard deviation of 17 %. Please note, that the cluster fractions were normalized with the overall footprint fraction within the test site. The area covered by the loamy cluster is 32 % of the test site area, which points to a potential under-representation of fluxes from the loamy cluster area using the EC method, see Fig. S9 on the spatial distribution of the average footprint weight in the supplementary material. Depending on the temporal persistence and the magnitude in differences between NEE originating either from the loamy or the stony area of the test site, this may induce biased estimates of NEE based on the EC method. In order to test this, we combined the footprint model with the agroecosystem model. In a first step we assumed that the 'true' spatial average hourly NEE of the test site is the sum of the AgroC model ensemble mean NEE of the loamy and the stony cluster weighted by the respective areal fraction of each cluster. The two areal fractions are constant over time and the model ensemble of the loamy cluster is the average of the hourly NEE estimated for locations p1, p2, p4, p6, p10, p11, p12, p15 and p18. The stony cluster AgroC average NEE was calculated from the model results at locations p3, p5, p7, p8, p9, p13, p14, p16 and p17. In the second step we scaled the hourly stony and loamy cluster ensemble NEE with the respective hourly flux footprint weight computed for the loamy and the stony area as describe above. Figure 10 shows the area-weighted NEE, the footprint weighted NEE and the difference between both fluxes computed as area-weighted mean minus footprint-weighted mean. For graphic representation in Fig. 10 the hourly fluxes were aggregated to daily fluxes. At this point, the difference between area-weighted and footprint-weighted fluxes is the

only result of the space and time variable flux footprint covering the loamy and the sandy cluster area to a different degree. As expected from the footprint analyses the loamy area is slightly under-represented, which causes a negative bias. The footprint-weighted fluxes are slightly less negative because the fluxes originating from the stony area, which dominate the flux footprint, are on average less negative in relation to the fluxes from the loamy cluster area. Averaged over the entire observation period the bias is -10 mol CO_2 ha^{-1} h^{-1}, with a standard deviation of 17 mol CO_2 ha^{-1} h^{-1}. In relation to the observation period area-averaged NEE of -177 mol CO_2 ha^{-1} h^{-1} this amounts to 5.6 %. The most negative deviation of -81 mol CO_2 ha^{-1} h^{-1} was observed for March 23, 2016. We further assumed that a potential bias will be larger during the dry period. Due to larger differences in NEE, as a consequence of increasing differences in root water uptake stress between the stony and the loamy parts of the test site, a bias would increase. In absolute terms, the bias during the summer period without stress (May 25 to August 24) was -16 mol CO_2 ha^{-1} h^{-1}, whereas the bias during the stress period (August 25 to September 30) was -11 mol CO_2 ha^{-1} h^{-1}. However, in relation to the area-weighted NEE averaged for the same periods, this represents a relative deviation of 4.6 % for the non-stressed summer period and 14.4 %, and thus indeed a larger relative bias, for the water stress period.

4. Discussion

4.1 Point-scale chamber measurements vs. eddy covariance data

NEE and soil respiration measured at site F01 was similar in magnitude and seasonal variability to those measured at other comparable sugar beet sites (Aubinet et al., 2009; Buysse et al., 2017; Moureaux et al., 2006; Burkart et al., 2009). Burkart et al. (2007), for example, measured daily peak NEE values of about -40 μmol m^{-2} s^{-1} (=-1440 mol CO_2 ha^{-1} h^{-1}) at a sugar beet site near Braunschweig, Germany, during July 2001, which corresponds well to our July measurements of NEE in 2016, based on either the chamber or the EC method (Fig. 2). Our

study also confirms that chamber-based measurements of NEE (Langensiepen et al., 2012; Graf et al., 2013) are important tools, because they are basically appropriate to measure point-scale NEE fluxes. The chamber technique on the other hand has practical limitations. The 18 chamber-based measurements took about 2 hours, which is a time limit imposed, when measurements should characterize the spatial variability. For which, in a very strict sense, measurements at exactly the same time would be required. This clearly limits the number of sampling locations and introduces uncertainty to the chamber-based patterns of NEE. As shown in this study, in practice this works out reasonably well, given that unstable radiation conditions of partially clouded skies were omitted, that would have caused oscillating intervals of direct sunshine and shaded conditions due to a cloud, and revisiting times were long enough (Langensiepen et al., 2012). Further, the deviations between EC and chamber NEE could be explained to some extent by the different time scales of the methods. The 'snapshot character', i.e. NEE chamber closure time is two minutes, and the procedure of sequential chamber measurements at the 18 sampling locations within a ~two-hour time window raises some uncertainty when related to the hourly average flux measured by the EC method at noon.

The agreement between the chamber-measured and the EC-based NEE is good and the correlation between EC-based NEE and chamber measurements is comparable to what was observed e.g. by Graf et al. (2013). However, during the period after Aug 25 the chamber method shows constantly more negative fluxes than the EC data. The flux footprint analysis revealed that this is potentially related to the fact that the more negative fluxes from the loamy areas of the test site are under-represented by the EC method, as reported in section 3.5. Even before emergence of the sugar beet crops within F01 negative NEE was observed by the EC method, which might be a consequence of the fact that a certain fraction of the flux footprint outside of F01 was cropped with photosynthetically active winter wheat at that time (Brogi et

al., 2020). The total fraction of the footprint outside of F01 however was on average less than 28 %.

4.2 Temporal stability and spatial analysis of NEE and soil respiration

Stadler et al. (2015) observed that the within-field crop growth heterogeneity changed during the growing period. In this study also coefficients of variation changing over time were observed for NEE. Stadler et al. (2015) further observed that in dry years patterns of soil physical properties had a pronounced influence on crop growth. This is also corroborated by this study, since the highest spatial variation in NEE was observed during the period of severe water stress. We also observed an increase in the spatial variation of NEE from July 2016 on. This could be explained by the effect of root water uptake stress on instantaneous assimilation (Kupisch et al., 2015). It can also be the result of a cumulative process, since the plants growing constantly under favorable soil water availability conditions will show higher photosynthetic activity, resulting in more biomass and LAI on average, in relation to sites with a constantly lower soil water availability (Hakojärvi et al., 2013). The discrepancies between the two extreme settings would thus be expected to increase over the vegetation period.

The spatial variation in soil respiration also increases over time. Since the within-field variation of soil temperatures was low (data not shown), this is probably the consequence of two factors related to soil water content. The first one is the direct effect of soil water content on the heterotrophic respiration activity. The spatial variation of soil moisture increases over the vegetation period as the stony patches loose soil water faster than the loamy patches (see Fig. 5), thus creating larger discrepancies in soil water content within the field, which in turn generates a higher variation in heterotrophic soil respiration. The second factor is related to the indirect effect of soil water availability on crop growth. At the loamy patches crop growth is stronger, which would induce higher biomass in the roots and higher autotrophic soil

respiration, whereas lower autotrophic respiration rates would be given for the stony patches with lower root biomass. Again, these effects would be expected to be stronger towards the end of the growing period, when spatial variation in soil water content is high. The spatial CV of soil respiration was on average lower than for NEE, and the overall levels of variation were comparable to the observations of e.g. Herbst et al. (2012) for bare soil and Prolingheuer et al. (2014) for a winter wheat stand.

For EC-based measurements of NEE in agricultural settings our findings on the temporal evolution of spatial variation in soil respiration and NEE indicate increasing uncertainties over the growing period and highest uncertainties in periods with severe root water uptake stress. In this study, we detected spatial CVs of NEE up to 0.72, which probably represents a magnitude that could cause bias in case the flux footprint shows unfavorable non-representative spatial coverage, e.g. by swinging between areas that are characterized by severe root water uptake stress and unstressed areas. This, of course, only plays a role when the underlying spatial pattern shows a high degree of spatial organization (i.e. deterministic) and not just a random pattern. In this respect, the site investigated in this study clearly represents a 'worst case' scenario, where the paleo-channel pattern is not only deterministic but it is also characterized by a high diversity of soil properties impacting the crop photosynthetic activity. The within-field CVs of NEE observed in this study are also higher than those observed by Hakojärvi et al. (2013) for the biomass of spring wheat and spring barley at harvest, ranging between 0.04 and 0.34. Stadler et al. (2015) measured biomass CVs of 0.24 and 0.17 at two sites located very close to the test site investigated in this study. The average within-field CVs of yield recorded by Joernsgard and Halmoe (2003) for a suite of sites located in the UK and Denmark, years, and crops varied between 0.10 and 0.18. All these numbers are lower than the CVs detected in this study for NEE, mainly for two reasons. First, instantaneous fluxes measured in this study are expected to vary over time, whereas the CVs related to biomass at harvest represent a cumulative value

over time. The second reason is the already mentioned above-average variability of soil properties observed for our test site F01.

4.3 Modeling of water stress at the two intensively monitored sites

The modelling of the two extreme locations p2 and p16 shows that root water uptake stress is the limiting factor for crop growth within F01, as documented in various studies (Kupisch et al., 2015; Hakojärvi et al., 2013), particularly for sugar beet (Freckleton et al., 1999; Richter et al., 2001; Tognetti et al., 2003; Hoffmann and Kenter, 2018; Fitters et al., 2018). The models established for p2 and p16 allow the quantification of the effect of water stress on NEE and yield. For location p2 very little water stress was estimated (top panel Fig. 5) resulting in an estimated sugar beet yield of ~15 t dry mass ha^{-1}. At the highly stressed location p16 a reduced yield of ~9 t dry mass ha^{-1} was estimated. In relation to the maximum potential yield of 31 t dry mass ha^{-1}, reported by Hoffmann and Kenter (2018), even the relatively unstressed location p2 produces a beet yield of only half of that value. However, the authors stress that such a high yield can probably only be achieved by additional water supply by irrigation. From this study we deduce that, apart from sufficient nutrient supply of course, also the soil profile must have perfect soil hydraulic properties too, in order to store and provide the water for root uptake. Of course, not only the beet yield was affected by root water uptake stress, also biomass and LAI development were impacted. Tognetti et al. (2003) observed increases in LAI over the sugar beet growing season for a sprinkler irrigated treatment varying between 0.5 and 1.5 in relation to a non-irrigated control plot, which is resembled by the measured and simulated differences in LAI between p2 and p16 (Fig. 6).

The plant parameter input for p2 and p16 was identical, except for the assimilate partitioning factors to root and shoot, further referred to as the root/shoot ratio. This was required for an optimum simulation of biomass, LAI, and NEE at the two locations. The underlying assumption

was that for root water uptake stressed situations the crop provides more assimilates to the fibrous root system, as the leaf area is not the main limiting factor for photosynthetic yield. This was experimentally observed by Fitters et al. (2018) and Tognetti et al. (2003). In terms of modelling this basically mimics a feedback process by which drought stress affects crop physiology regarding the root/shoot ratio. This feedback appears to be relevant for a sound estimation of the effects of drought on sugar beet yield. However, this process is currently not implemented in any of the commonly applied mechanistic crop models like e.g. AquaCrop (Raes et al., 2017), MONICA (Nendel et al., 2011), or WOFOST (Boogaard et al., 2014).

According to the cluster analysis, the paleo channel system occupies 32% of the entire test field. Computing an average estimated NEE weighted according to the spatial fractions, assuming that the p2 model is representative for the paleo channel part and the p16 model is representative for the fluxes from the region outside the channels, improves agreement to the EC data. The ME between the weighted model average and the EC-based measurements increases to a value of 0.86, which points to a clear improvement in relation to the agreement of each single model to the EC data (see Table 2).

4.4 Reproduction of spatio-temporal features with the model

Based on the models derived for p2 and p16, additional models were established for the other 16 locations, which differ in profile geometry, soil hydraulic properties, and soil organic carbon pools. Based on this setup, the model was able to reproduce the temporal evolution of NEE at each location, as measured by chambers, as well as the spatial patterns in terms of the average fluxes at all locations. Each of the 18 models is characterized by a specific set of soil hydraulic parameters, which in turn generate the root water uptake stress pattern over time and space. This clearly identifies the root water uptake stress as the main driver of spatial variability in CO_2 flux within F01. The relation between the chamber-measured average NEE at the sampling

points and the root water uptake stress was corroborated by calculating the soil water storage capacity S_{WSC} for the Ap and B horizon (Table 3). At each sampling location the maximum volume of water that could be stored in the soil above the gravel layers, S_{WSC}, was calculated from the measured water content at saturation (Table S3 supplementary material) and the respective layer thickness (Table S2 supplementary material). The spatial correlation coefficient between chamber-measured NEE and S_{WSC} was -0.67. This points to very negative NEE at locations with high S_{WSC} and this further supports the identification of the massive effect of root water uptake stress on point-scale NEE as it was described by the model.

The agreement of NEE in terms of spatial and temporal variation between chamber measurements and the model ensemble was of course not perfect. The model ensemble variation of NEE over time was lower than measured by the chambers during the first half of the growing period, without severe water stress. The increase in NEE spatial variability during the dry period was reproduced by the model, which is a relevant feature. However, the variability predicted by the model was also lower than the chamber observations (see Fig. 2 and Fig. 9). Parts of the chamber-based variation in NEE are the result of measurement errors and uncertainties related to basic technical issues (Langensiepen et al., 2012) and to the 2h duration of each chamber measurement campaign. Most of the difference is probably attributed to deficits in the model setup in terms of parameters and processes. The model ensemble members do not differ in the plant parameters, except for the root/shoot ratios of either p2 or p16, as discussed in the previous section. This probably does not cover the natural variability of crop growth and development. Further, either the parametrization of p2 or p16 is used to account for the effect of drought stress on the root/shoot ratio, but there is no dynamic feedback process related to the water stress estimated at a specific location or model ensemble member. This would introduce more variability in the model ensemble estimated variability of NEE. The implementation of such a dynamic feedback of drought stress on crop physiology for sugar beet

seems highly relevant, but it would require a dedicated experimental dataset with various degrees of root water uptake stress to derive such an algorithm.

4.5 Uncertainty arising from spatial variation in NEE

For the estimation of a potential bias in NEE determined by the EC method we assumed that the AgroC simulated NEE weighed by the areal fractions of the loamy and the stony parts of the test site, represent the 'true' NEE. The real NEE of test site F01 will inherently differ from the agroecosystem model estimates. However, this difference appears to be rather small, since the coefficient of determination between the EC data and the area-weighted AgroC NEE is 0.87. The slope and intercept of the regression equation are 1.02 and -14 mol CO_2 ha^{-1} h^{-1}, pointing to little bias of the AgroC estimates in relation to the EC data. Notably, the EC data was not used to calibrate the agroecosystem model. Another relevant point is that the differences between the AgroC estimated NEE of the loamy and sandy cluster has to be realistic. The evaluation of the model performance for the sandy and the loamy cluster averages against the chamber data shows good agreement of the timing and overall magnitude of estimated NEE (see end of section 3.4).

The combination of the flux footprint model with the agroecosystem model actually reveals a bias related to the underlying spatial pattern of soil properties which affect the sugar beet assimilation activity and thus create a spatial pattern in NEE. However, over the vegetation period this effect appears to be rather small (see Fig. 10), particularly in relation to the magnitude of the average NEE, which points to a systematic underestimation of NEE by 5.6 %. During the period of severe water stress a 2.6 times higher bias (14.4 %) was estimated. However, this is related to a period of 37 days only. The overall uncertainty associated to this effect of within-field spatial patterns of NEE on EC-based field average NEE is even lower than other uncertainties, typically on an order of magnitude of 20 % of the measured flux, like

the energy balance closure (Hendricks-Franssen et al., 2010) or random uncertainty and errors due to measurement devices and turbulence (Hollinger and Richardson, 2005; Mauder et al., 2013; Post et al., 2015). The year 2016 was a rather average year in hydroclimatic conditions. For more extreme conditions like severe drought, associated with sustained water stress periods, the bias would increase.

5. Conclusions

The chamber technique is a valid complement to the EC method, particularly when the test site is characterized as heterogeneous or patchy. The good agreement between AgroC estimated NEE and EC-based NEE indicates a potential use of the agroecosystem model for gap-filling, explicitly for water stress periods. We further conclude that the implementation of a feedback process between root water uptake stress and plant physiology could improve NEE and sugar beet yield estimates. The chamber-based measurements of NEE reveal that high spatial coefficients of variation were present during drought and appear to be high enough to distort fluxes measured by the eddy covariance method. However, the combination of the flux footprint model with the agroecosystem model revealed that despite severe within-field spatial heterogeneity in NEE the spatial averaging effect of the EC method is large enough to generate only little bias in the EC-based NEE, which is more pronounced for periods with root water uptake stress. This clearly also has to be seen against the background of the high spatial variability of soil properties affecting point-scale NEE at the field investigated in this study. We further conclude that the characteristic length, i.e. the spatial scale, of the spatial pattern in NEE has to be considerably smaller than the characteristic length of the flux footprint to guarantee a bias-free EC application.

Acknowledgements

This study was supported by the Deutsche Forschungsgemeinschaft through the "Transregional Collaborative Research Center 32 - Patterns in Soil–Vegetation–Atmosphere Systems: Monitoring, Modeling and Data Assimilation". This research was partially funded by the Deutsche Forschungsgemeinschaft (DFG, German Research Foundation) under Germany's Excellence Strategy - EXC 2070 – 390732324. The authors also like to thank Bernd Schilling and Ansgar Weuthen for installation and maintenance of the SoilNet, Daniel Dolfus and Nicole Adels for set up and maintenance of the EC tower and Anke Langen for laboratory assistance.

References

Allen, R.G., Pereira, L.S., Raes, D., Smith, M., 1998. Crop Evapotranspiration. Guidelines for computing crop water requirements. In: FAO Irrigation andDrainage Paper No. 56. Food and Agriculture Organization of the UnitedNations (FAO), Rome, 300 pp.

Aubinet, M., Moureaux, C., Bodson, B., Dufranne, D., Heinesch, B., Suleau, M., Vancutsem, F., Vilret, A., 2009. Carbon sequestration by a crop over a 4-year sugar beet/winter wheat/seed potato/winter wheat rotation cycle. Agricultural and Forest Meteorology 149, 407-418.

Baldocchi, D., 2014. Measuring fluxes of trace gases and energy between ecosystems and the atmosphere - the state and future of the eddy covariance method. Global Change Biology 20, 3600-3609.

Bauer, J., Weihermüller, L., Huisman, J.A., Herbst, M., Graf, A., Sequaris, J.M., Vereecken, H., 2012. Inverse determination of soil heterotrophic respiration dependency on temperature and water content under field conditions. Biogeochemistry 108, 119-134. DOI 10.1007/s10533-011-9583-1

Bogena, H.R., Herbst, M., Huisman, J.A., Rosenbaum, U., Weuthen, A., Vereecken, H., 2010. Potential of wireless sensor networks for measuring soil water content variability. Vadose Zone Journal 9, 1002–1013.

Boogaard, H.L, De Wit, A.J.W., te Roller, J.A., Van Diepen, C.A., 2014. WOFOST CONTROL CENTRE 2.1; User's guide for the WOFOST CONTROL CENTRE 2.1 and the crop growth simulation model WOFOST 7.1.7. Wageningen (Netherlands), Alterra, Wageningen University & Research Centre.

Brakensiek, D.L., Rawls, W.J., 1994. Soil containing rock fragments: effects on infiltration. Catena 23, 99–110.

Brogi, C., Huisman, J.A., Pätzold, S., von Hebel, C., Weihermüller, L., Kaufmann, M.S., van der Kruk, J., Vereecken, H., 2019. Large-scale soil mapping using multi-configuration EMI and supervised image classification. Geoderma, 335, 133-148. doi.org/10.1016/j.geoderma.2018.08.001

Brogi, C., Huisman, J.A., Herbst, M., Weihermüller, L., Klosterhalfen, A., Montzka, C., Reichenau, T.G., Vereecken, H., 2020. Simulation of spatial variability in crop LAI and yield using agro-ecosystem modelling and geophysics-based quantitative soil information. Vadose Zone Journal 19, e20009. https://doi.org/10.1002/vzj2.20009

Brown, K.F., Briscoe, P.V., 1985. Fibrous root growth and water use of sugar beet. J. Agric. Sci. 105, 679-691.

Burkart, S., Manderscheid, R., Weigel, H.-J., 2007. Design and performance of a portable gas exchange chamber system for CO_2- and H_2O-flux measurements in crop canopies. Environmental and Experimental Botany 61, 25-34.

Burkart, S., Manderscheid, R., Weigel, H.-J., 2009. Canopy CO_2 exchange of sugar beet under different CO_2 concentrations and nitrogen supply: results from a free-air CO_2 enrichment study. Plant Biology 11, 109-123.

Buysse, P., Bodson, B., Debacq, A., De Ligne, A., Heinesch, B., Manise, T., Moureaux, C., Aubinet, M., 2017. Carbon budget measurement over 12 years at a crop production site in the silty-loam region in Belgium. Agricultural and Forest Meteorology 246, 241-255.

Cai, G., Vanderborght, J., Couvreur, V., Mboh, C.M., Vereecken, H., 2017. Parameterization of root water uptake models considering dynamic root distributions and water uptake compensation. Vadose Zone J.17:160125. doi:10.2136/vzj2016.12.0125

Chung, S.O., Horton, R., 1987. Soil heat and water-flow with a partial surface mulch. Water Resour. Res. 23(12), 2175–2186.

Coleman, K., Jenkinson, D.S., 2005. RothC-26.3. A Model for Turnover of Carbon in Soil, Model Description and Windows Users Guide. IACR-Rothamsted, Harpenden, 45 pp. http://www.rothamsted.bbsrc.ac.uk/aen/carbon/rothc.htm.

Davis, P.A., Clifton Brown, J., Saunders, M., Lanigan, G., Wright, E., Fortune, T., Burke, J., Connolly, J., Jones, M.B., Osborne, B., 2010. Assessing the effects of agricultural management practices on carbon fluxes: Spatial variation and the need for replicated estimates of Net Ecosystem Exchange. Agricultural and Forest Meteorology 150, 564-574. DOI: 10.1016/j.agrformet.2010.021

DIN ISO 11277, 2002. Bodenbeschaffenheit - Bestimmung der Partikelgrößenverteilung in Mineralböden - Verfahren mittels Siebung und Sedimentation (ISO 11277:1998 + ISO 11277:1998 Corrigendum 1:2002). English title: Soil quality - Determination of particle size distribution in mineral soil material - Method by sieving and sedimentation (ISO 11277:1998 + ISO 11277:1998 Corrigendum 1:2002)

Duan, Q.Y., Sorooshian, S., et al., 1992. Effective and efficient global optimization for conceptual rainfall-runoff models. Water Resour. Res. 28(4), 1015-1031.

Feddes, R.A., Kowalik, P.J., Zaradny, H., 1978. Simulation of field water use and crop yield. In: Simulation Monographs, Wageningen, p. 188.

Fitters, T.F.J., Mooney, S.J., Sparkes, D.L., 2018. Sugar beet root growth under different watering regimes: A minirhizotron study. Environmental and Experimental Botany 155, 79-86.

Freckleton, R.P., Watkinson, A.R., Webb, D.J., Thomas, T.H., 1999. Yield of sugar beet in relation to weather and nutrients. Agricultural and Forest Meteorology 93, 39-51.

Graf. A., Werner, J., Langensiepen, M., van de Boer, A., Schmidt, M., Kupisch, M., Vereecken, H., 2013. Agricultural and Forest Meteorology 174-175, 1-14. http://dx.doi.org/10.1016/j.agrformet.2013.02.001

Hakojärvi, M., Hautala, M., Ristolainen, A., Alakukku, L., 2013. Yield variation of spring cereals in relation to selected soil physical properties on three clay soil fields. Europ. J. Agronomy 49, 1-11.

Hendricks-Franssen, H.J., Stöckli, R., Lehner, I., Rotenberg, E., Seneviratne, S.I., 2010. Energy balance closure of eddy-covariance data: A multisite analysis for European FLUXNET stations. Agricultural and Forest Meteorology 150, 1553-1567. doi:10.1016/j.agrformet.2010.08.005

Herbst, M., Hellebrand, H.J., Bauer, J., Huisman, J.A., Simunek, J., Weihermüller, L., Graf, A., Vanderborght, J., Vereecken, H., 2008. Multiyear heterotrophic soil respiration: evaluation of a coupled CO_2 transport and carbon turnover model. Ecological Modelling 214, 271–283.

Herbst, M., Bornemann, L., Graf, A., Welp, G., Vereecken, H., Amelung, W., 2012. A geostatistical approach to the field-scale pattern of heterotrophic soil CO_2 emission using covariates. Biogeochemistry 111, 377-392. doi: 10.1007/s10533-011-9661-4

Hoffmann, C.M., Kenter, C., 2018. Yield potential of sugar beet – have we hit the ceiling? Frontiers in Plant Science 9, 289. http://dx.doi.org/10.3389/fpls.2018.00289

Hollinger, D.Y., Richardson, A.D., 2005. Uncertainty in eddy covariance measurements and its application to physiological models. Tree Physiology 25. 873-885.

IUSS Working Group WRB, 2007. World reference base for soil resources 2006, first update 2007. World Soil Resources Reports No. 103. FAO, Rome.

Joernsgaard, B., Halmoe, S. 2003. Intra-field yield variation over crops and years. Europ. J. Agronomy 19, 23-33.

Klosterhalfen, A., Herbst, M., Weihermüller, L., Graf, A., Schmidt, M., Stadler, A., Schneider, K., Subke, J.-A., Huisman, J.A., Vereecken, H., 2017. Multi-site calibration and

validation of a net ecosystem carbon exchange model for croplands. Ecological Modelling 363, 137-156. http://dx.doi.org/10.1016/j.ecolmodel.2017.07.028
Kormann, R., Meixner, F., 2001. An analytical footprint model for non-neutral stratification, Boundary Layer Meteoroly 99, 207–224. https://doi.org/10.1023/A:1018991015119
Kupisch, M., Stadler, A., Langensiepen, M., Ewert, F., 2015. Analysis of spatio-temporal patterns of CO_2 and H_2O fluxes in relation to crop growth under field conditions. Field Crops Research 176, 108-118.
Kutsch, W., Liu, C., Hörmann, G., Herbst, M., 2005. Spatial heterogeneity of ecosystem carbon fluxes in a broadleaved forest in northern Germany. Global Change Biology 11, 77-80.
Langensiepen, M., Kupisch, M., van Wijk, M.T., Ewert, F., 2012. Analyzing transient closed chamber effects on canopy gas exchange for optimizing flux calculation timing. Agricultural and Forest Meteorology 164, 61-70.
Mauder, M., Foken, T., 2011. Documentation and instruction manual of the Eddy covariance software package TK3, Univ.Bayreuth, Abt. Mikrometeorologie, 2011.
Mauder, M., Cuntz, M., Drüe, C., Graf, A., Rebmann, C., Schmid, H.-P., Schmidt, M., Steinbrecher, R., 2013. A quality assessment strategy for long-term eddy-covariance measurements. Agric. For. Meteorol. 169, 122-135.
Minasny, B., Malone, B.P., McBratney, A.B., Angers, D., Arrouays, D., et al., 2017. Soil carbon 4 per mille. Geoderma 292, 59-86.
Moureaux, C., Debacq, A., Bodson, B., Heinesch, B., Aubinet, M., 2006. Annual net ecosystem carbon exchange by a sugar beet crop. Agricultural and Forest Meteorology 139, 25-39.
Nash, J.E., Sutcliffe, J.V., 1970. River flow forecasting through conceptual models part I - A discussion of principles. J. Hydrol. 10(3), 282-290.
Nendel, C., Berg, M., Kersebaum, K.C., Mirschel, W., Specka, X., Wegehenkel, M., Wenkel, K.O., Wieland, R., 2011. The MONICA model: Testing predictability for crop growth, soil moisture and nitrogen dynamics. Ecol. Model. 222, 1614–1625.
Petrone, R.M., Chahil, P, Macrae, M.L., English, M.C., 2008. Spatial variability of CO_2 exchange for riparian and open grasslands within a first-order agricultural basin in Southern Ontario. Agriculture, Ecosystems and Environment 125, 137-147.
Post, H., Hendricks Franssen, H.J., Graf, A., Schmidt, M., Vereecken, H. 2015. Uncertainty analysis of eddy covariance CO_2 flux measurements for different EC tower distances using an extended two-tower approach. Biogeosciences 12, 1205-1221. doi:10.5194/bg-12-1205-2015
Prolingheuer, N., Scharnagl, B., Graf, A., Vereecken, H., Herbst, M, 2014. On the spatial variation of soil rhizospheric and heterotrophic respiration in a winter wheat stand. Agricultural and Forest Meteorology 195-196, 24-31. DOI: 10.1016/j.agrformet.2014.04.016
Raes, D., Steduto, P., Hsiao, T.C., Fereres, E., 2017. Reference manual AquaCrop version 6.0, FAO. Rome.
Rawls, W.J., Brakensiek, D.L., 1985. Prediction of soil water properties for hydrologic modelling. American Society of Civil Engineers, 293–299.
Richter, G.M., Jaggard, K.W., Mitchell, R.A.C., 2001. Modelling radiation interception and radiation use efficiency for sugar beet under variable climatic stress. Agricultural and Forest Meteorology 109, 13-25.
Riutta, T., Laine, J., Aurela, M., Rinne, J., Vesala, T., Laurila, T., Haapanala, S., Pihlatie, M., Tuittila, E.-S., 2007. Spatial variation in plant community functions regulates carbon gas dynamics in a boreal fen ecosystem. Tellus 59B, 838-852.
Rudolph, S., van der Kruk, J., Von Hebel, C., Ali, M., Herbst, M., Montzka, C., Pätzold, S., Robinson, D., Vereecken, H., Weihermüller, L., 2015. Linking satellite derived LAI

patterns with subsoil heterogeneity using large-scale ground-based electromagnetic induction measurements. Geoderma 241, 262-271.
Simunek, J., Suarez, D.L., 1993. Modeling of carbon dioxide transport and production in soil 1. Model development. Water Resources Research 29(2), 487–497. http://dx.doi.org/10.1029/92WR02225
Spitters, C.J.T., van Keulen, H., van Kraalingen, D.W.G., 1989. A simple and universal crop growth simulator, SUCROS87. In: Rabbinge, R., Ward, S.A., van Laar, H.H.(Eds.), Simulation and Systems Management in Crop Protection. Simulation Monographs 32. PUDOC, Wageningen, pp. 147–181.
Stadler, A., Rudolph, S., Kupisch, M., Langensiepen, M., van der Kruk, J., Ewert, F., 2015. Quantifying the effects of soil variability on crop growth using apparent soil electrical conductivity measurements. Europ. J. Agronomy 64, 8-20.
Tognetti, R., Palladino, M., Minnocci, A., Delfine, S., Alvino, A., 2003. The response of sugar beet to drip and low-sprinkler irrigation in southern Italy. Agricultural Water Management 60, 135-155.
Vachaud, G., Passerat De Silans, A., Balabanis, P., Vauclin, M., 1985. Temporal stability of spatially measured soil water probability density function. Soil Sci. Soc. Am. J. 49, 822-828.
Weihermüller, L., Graf, A., Herbst, M., Vereeecken, H., 2013. Simple pedotransfer functions to initialize reactive carbon pools of the RothC model. Eur. J. Soil Sci. 64, 567–575. http://dx.doi.org/10.1111/ejss.12036.

Table 1
Days between measurements and Pearson correlation coefficients *r* between consecutive net ecosystem exchange (NEE) and soil respiration (R_s) measurements.

Date 2016	Interval d	*r* NEE	Date 2016	Interval d	*r* R_s
25 May			19 May		
8 June	14	0.06	25 May	6	0.84
16 June	8	0.50	3 June	9	0.21
23 June	7	0.39	8 June	5	0.52
30 June	7	0.12	16 June	8	0.35
7 July	7	0.21	23 June	7	0.54
12 July	5	0.33	30 June	7	0.53
21 July	9	0.01	7 July	7	0.69
28 July	7	0.51	21 July	14	0.42
3 Aug	6	0.06	28 July	7	0.43
16 Aug	13	0.08	3 Aug	6	0.48
19 Aug	3	0.63	16 Aug	13	0.05
25 Aug	6	0.21	19 Aug	3	0.87
1 Sept	7	0.71	1 Sept	13	0.86
9 Sept	8	0.90	15 Sept	14	0.84
15 Sept	6	0.82	29 Sept	14	0.44
29 Sept	14	0.92	13 Oct	21	0.34
20 Oct	21	0.67			

Table 2
Mean absolute error MAE, root mean square error RMSE, model efficiency ME, coefficient of determination R^2 between measurement and AgroC model result on soil temperature T (subscripts refer to measurement depth in cm), soil water content θ (subscripts refer to measurement depth in cm), dry mass DM of sugar beet and leaves, green leaf area index LAI_g, brown leaf area index LAI_b, soil respiration R_s and net ecosystem exchange NEE for sites p2 and p16

		MAE	RMSE	ME	R^2
	unit		p2		
T_{10}	°C	1.059	1.313	0.88	0.89
T_{20}	°C	0.847	1.079	0.87	0.89
T_{50}	°C	1.209	1.484	0.60	0.74
θ_{10}	$cm^3\ cm^{-3}$	0.023	0.027	0.78	0.81
θ_{20}	$cm^3\ cm^{-3}$	0.019	0.023	0.88	0.88
θ_{50}	$cm^3\ cm^{-3}$	0.017	0.022	0.91	0.93
beet	DM t/ha	1.708	2.003	0.84	0.85
leaves	DM t/ha	0.872	0.977	0.70	0.71
LAI_g	-	0.251	0.301	0.93	0.94
LAI_b	-	0.136	0.193	0.06	0.21
R_s	mol CO_2 ha^{-1} h^{-1}	15.7	22.3	0.72	0.72
NEE	mol CO_2 ha^{-1} h^{-1}	117.3	170.8	0.79	0.82
			p16		
T_{10}	°C	2.002	2.703	0.71	0.76
T_{20}	°C	0.894	1.106	0.87	0.90
T_{50}	°C	1.185	1.485	0.68	0.84
θ_{10}	$cm^3\ cm^{-3}$	0.014	0.019	0.92	0.92
θ_{20}	$cm^3\ cm^{-3}$	0.008	0.011	0.98	0.98
θ_{50}	$cm^3\ cm^{-3}$	0.007	0.012	0.87	0.88
beet	DM t/ha	0.968	1.143	0.90	0.91
leaves	DM t/ha	0.405	0.458	0.65	0.66
LAI_g	-	0.347	0.445	0.74	0.83
LAI_b	-	0.148	0.260	-0.03	0.23
R_s	mol CO_2 ha^{-1} h^{-1}	24.7	33.8	0.61	0.61
NEE	mol CO_2 ha^{-1} h^{-1}	140.0	209.2	0.68	0.78

Table 3
Pearson correlation coefficient r over time between chamber-measured soil respiration R_s and net ecosystem exchange of carbon dioxide NEE with respective model results. Average fluxes of soil respiration at each sampling location of the chamber measurements $R_{s,avg,cham}$ and the model results $R_{s,avg,mod}$, average NEE at each sampling location of the chamber measurements $NEE_{av,cham}$ and model results $NEE_{av,mod}$ and soil water storage capacity S_{WSC}

	R_s r over time	$R_{s,avg,cham}$ mol CO_2 ha^{-1} h^{-1}	$R_{s,avg,mod}$ mol CO_2 ha^{-1} h^{-1}	NEE r over time	$NEE_{av,cham}$ mol CO_2 ha^{-1} h^{-1}	$NEE_{av,mod}$ mol CO_2 ha^{-1} h^{-1}	S_{WSC} mm
p1	0.60	90	72	0.64	-416	-566	203
p2	0.69	96	83	0.57	-625	-679	389
p3	0.70	88	112	0.65	-576	-473	214
p4	0.60	82	70	0.41	-609	-506	202
p5	0.62	75	91	0.68	-315	-393	111
p6	0.42	107	71	0.56	-621	-675	398
p7	0.63	123	113	0.52	-671	-522	423
p8	0.64	65	74	0.76	-515	-424	141
p9	0.67	86	101	0.76	-489	-479	209
p10	0.57	66	71	0.85	-691	-538	216
p11	0.62	108	72	0.47	-639	-594	284
p12	0.61	100	79	0.85	-760	-614	268
p13	0.82	109	102	0.85	-588	-441	208
p14	0.59	80	98	0.77	-564	-481	212
p15	0.71	103	66	0.70	-667	-548	270
p16	0.64	90	83	0.80	-363	-391	102
p17	0.78	91	88	0.62	-526	-390	151
p18	0.71	92	29	0.34	-497	-394	155
average	0.65	92	82	0.66	-563	-506	231

FIGURE CAPTIONS

Figure 1. Location of sampling points p1 to p18, eddy covariance tower location (EC) and apparent electrical conductivity EC_a at test site F01

Figure 2. a) hourly eddy covariance-based (EC) measurements of net ecosystem exchange of carbon dioxide NEE (points), average (lines with points) and standard deviations (shaded areas) of weekly to bi-weekly chamber-based measurements of NEE and soil respiration R_s. b) weekly to bi-weekly coefficient of variation of chamber-based NEE and R_s

Figure 3. Ranked mean relative differences in net ecosystem exchange NEE and soil respiration (R_s). Numbers in the graph refer to the sampling location. The right-hand plots show the location in the experimental site and apparent electrical conductivity EC_a.

Figure 4. Hourly eddy covariance-based (EC) measurements of net ecosystem exchange of carbon dioxide NEE (points), cluster average (lines with points) and cluster standard deviations (shaded areas) of weekly to bi-weekly chamber-based measurements of NEE and soil respiration R_s according to the loamy and the stony subset

Figure 5. top) Depth-specific simulated and measured soil water content θ at site p2 and p16 (middle). Bottom) dimensionless water stress factor at site p2 and p16.

Figure 6. top) measured (points) and simulated (lines) biomass of leaves and sugar beet at sites p2 and p16. Bottom) measured (points) and simulated (lines) leaf area index of green (LAI_{gre}) and brown (LAI_{bro}) leaves at sites p2 and p16.

Figure 7. top) hourly measured (points with error bars) and simulated (line) soil respiration R_s at site p2. Bottom) hourly measured (points with error bars) and simulated (line) soil respiration R_s at site p16. The error bars represent measurement standard deviation.

Figure 8. Eddy covariance-measured hourly net ecosystem exchange of carbon dioxide NEE (points) and model results for sites p2 and p16 (lines)

Figure 9. Hourly eddy covariance-based (EC) measurements of net ecosystem exchange of carbon dioxide NEE (points), weekly to bi-weekly AgroC ensemble average (lines with points) and standard deviations (shaded areas) of NEE and soil respiration R

Figure 10. Daily NEE estimated with AgroC from loamy cluster and stony cluster average flux weighted either according to the area covered by each cluster or according to the eddy covariance flux footprint weight within each cluster area. The difference is area-weighted minus footprint-weighted NEE.

Fig. 1

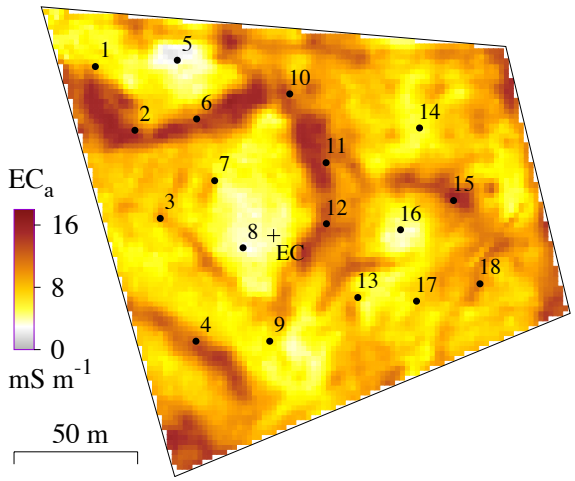
1
5
10
2
6
14
11
7
15
EC$_a$
3
12
16
8
+
EC
16
18
13
17
8
4
9
0
mS m^{-1}
50 m

Fig. 2

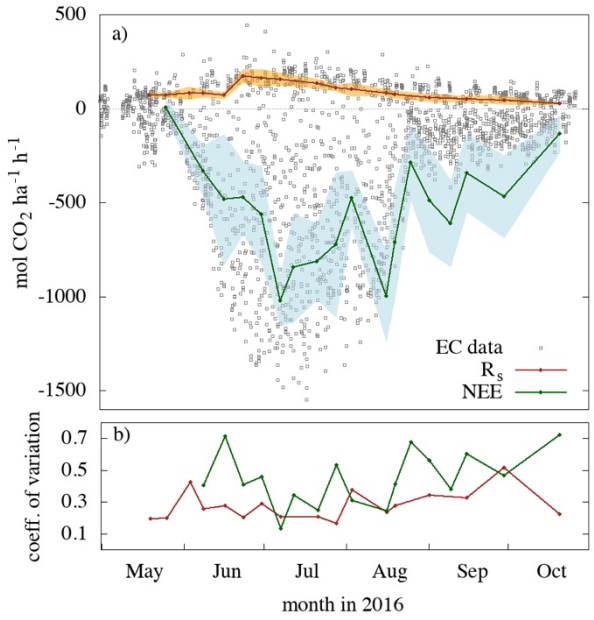
a)
500
0
-500
-1000
-1500
mol CO$_2$ ha^{-1} h^{-1}
EC data
R$_s$
NEE
b)
coeff. of variation
0.7
0.5
0.3
0.1
May
Jun
Jul
Aug
Sep
Oct
month in 2016

Fig. 3

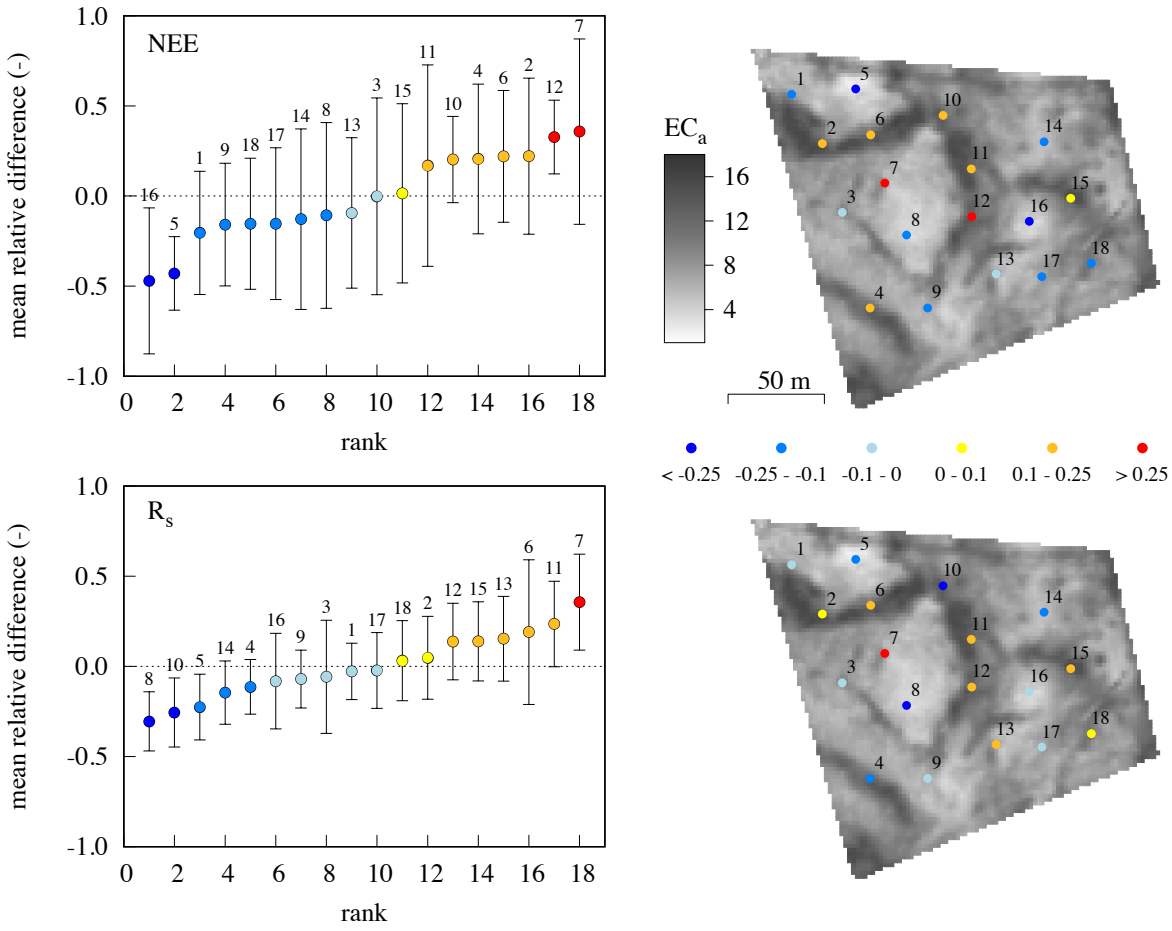
NEE
mean relative difference (-)
rank
1.0
0.5
0.0
-0.5
-1.0
0 2 4 6 8 10 12 14 16 18
16 5 1 9 18 17 14 8 13 3 15 11 10 4 6 2 12 7
R_s
8 10 5 14 4 16 9 3 1 17 18 2 12 15 13 6 11 7
EC_a
16
12
8
4
50 m
1 5 10 2 6 14 11 7 15 3 12 8 16 18 13 17 4 9
< -0.25
-0.25 - -0.1
-0.1 - 0
0 - 0.1
0.1 - 0.25
> 0.25

Fig. 4

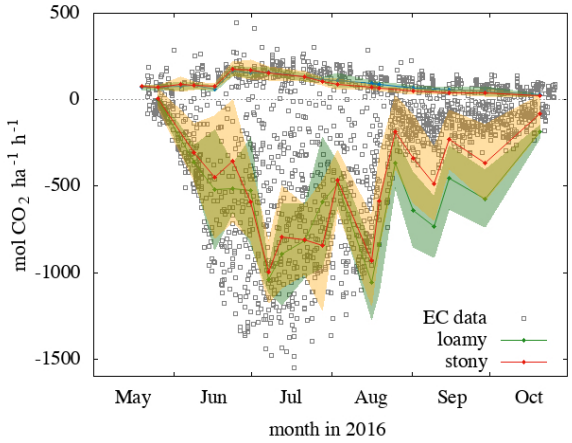
500
0
-500
-1000
-1500
mol CO2 ha-1 h-1
EC data
loamy
stony
May
Jun
Jul
Aug
Sep
Oct
month in 2016

Fig. 5

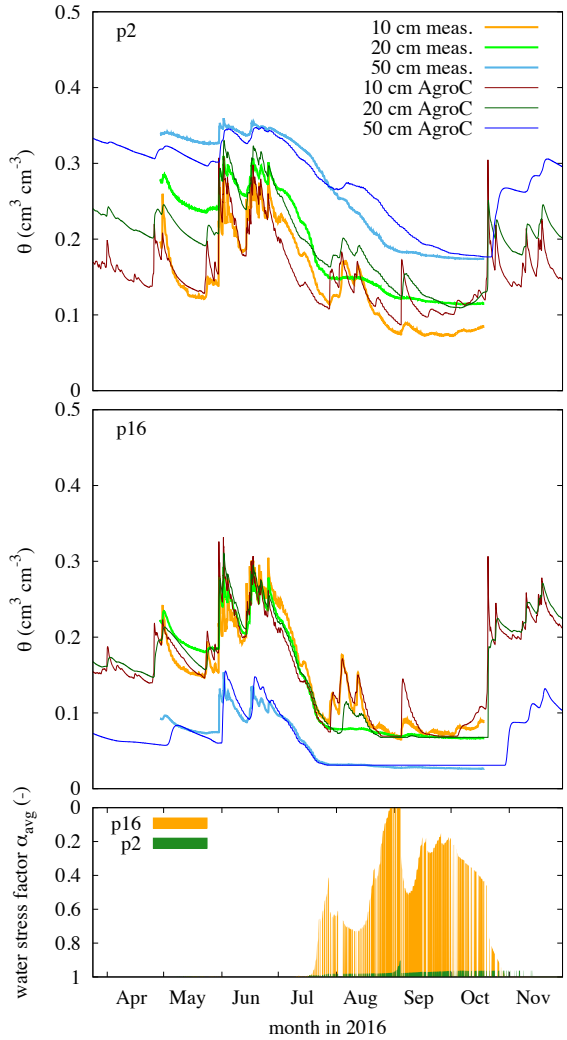
p2
10 cm meas.
20 cm meas.
50 cm meas.
10 cm AgroC
20 cm AgroC
50 cm AgroC
θ (cm3 cm-3)
p16
p16
p2
water stress factor αavg (-)
Apr
May
Jun
Jul
Aug
Sep
Oct
Nov
month in 2016

Fig. 6

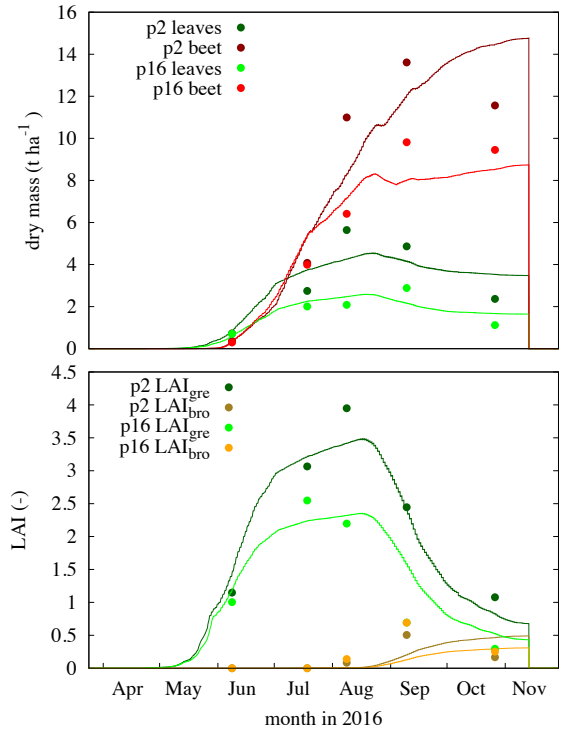
p2 leaves
p2 beet
p16 leaves
p16 beet
dry mass (t ha-1)
p2 LAIgre
p2 LAIbro
p16 LAIgre
p16 LAIbro
LAI (-)
Apr
May
Jun
Jul
Aug
Sep
Oct
Nov
month in 2016

Fig. 7

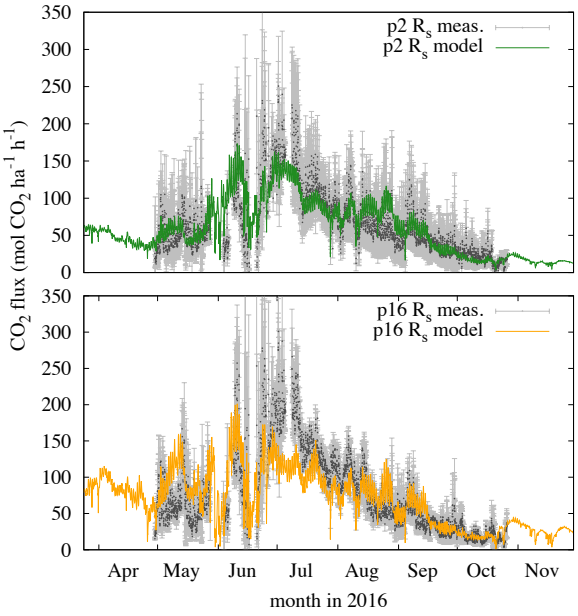
p2 Rs meas.
p2 Rs model
p16 Rs meas.
p16 Rs model
CO2 flux (mol CO2 ha-1 h-1)
Apr
May
Jun
Jul
Aug
Sep
Oct
Nov
month in 2016

Fig. 8

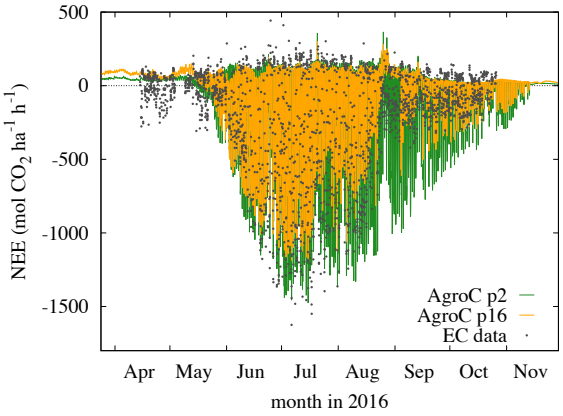

Fig. 9

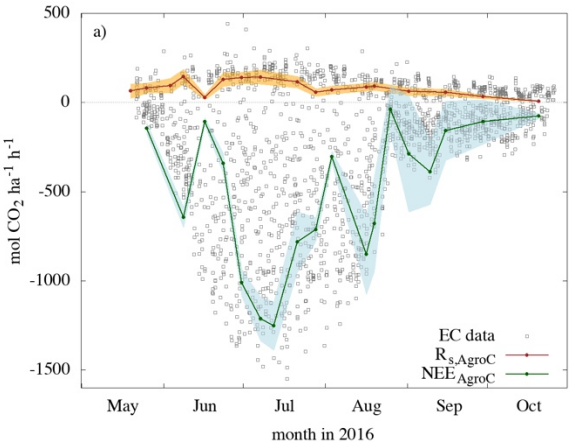

Fig. 10

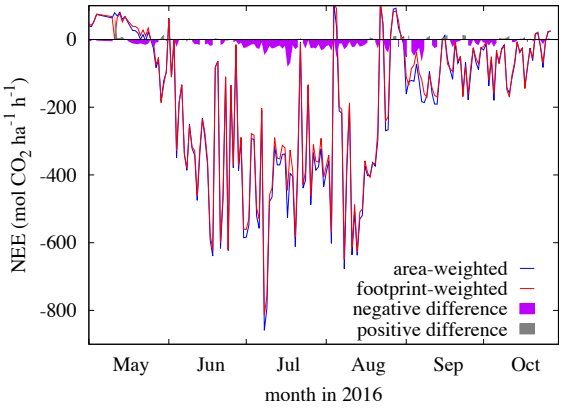

Fig. S1 Layering and coarse fraction of soil profiles

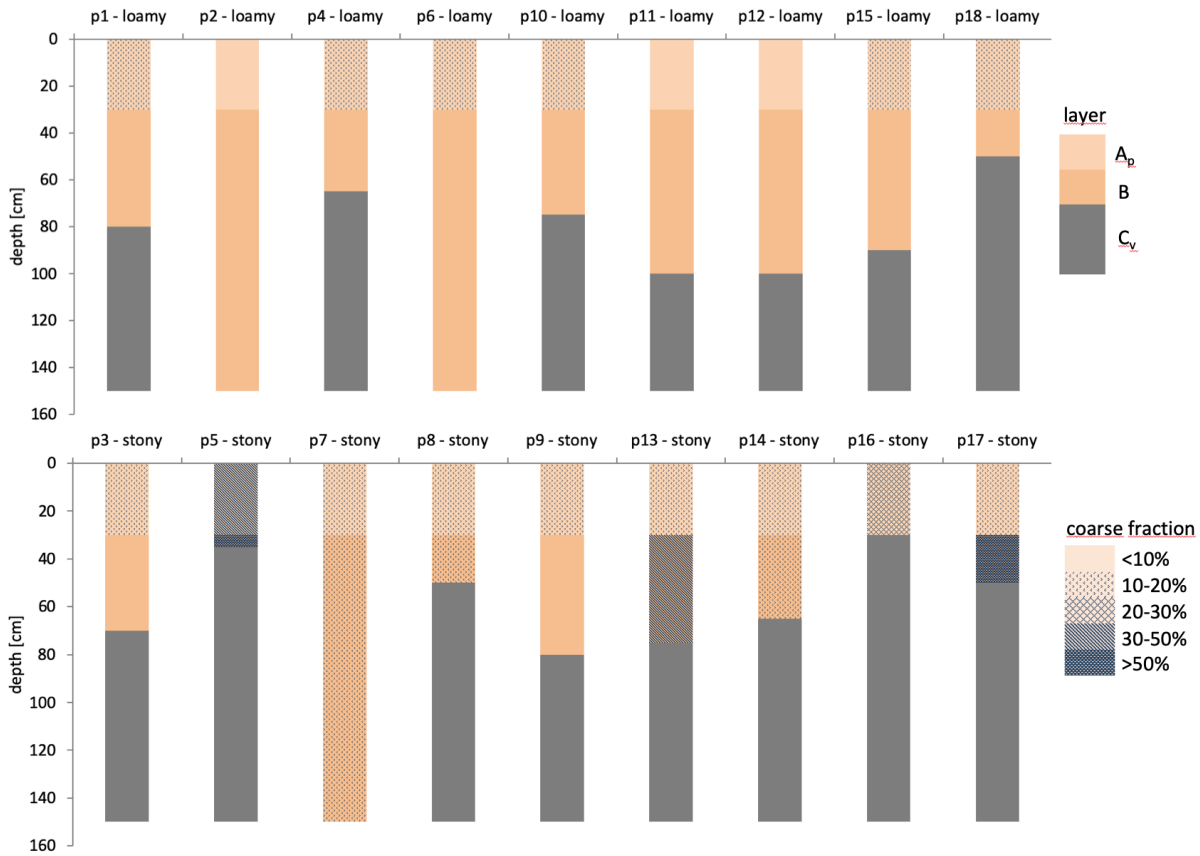

Table S2 Site-specific B horizon thicknes H_B, organic carbon content C_{org}, clay fraction C, silt fraction U, sand fraction S, bulk density ρ, and volumetric coarse fraction X (> 2mm). Subscripts Ap and B refer to the Ap and the B horizon respectively. Please note that for p16 bulk density and coarse fraction provided for the B horizon actually refer to the gravel layer Cv.

site	H_B	C_{orgAp}	C_{orgB}	C_{Ap}	U_{Ap}	S_{Ap}	C_B	U_B	S_B	ρ_{Ap}	ρ_B	X_{Ap}	X_B
	cm	%	%	%	%	%	%	%	%	g cm^{-3}	g cm^{-3}	%vol	%vol
p1	50	1.03	0.37	15.2	67.5	17.3	20.7	61.8	17.6	1.52	1.62	9.8	5.2
p2	125	1.04	0.55	14.7	61.9	23.4	22.6	54.1	23.3	1.41	1.53	3.7	2.3
p3	40	1.13	0.78	10.3	66.0	23.7	14.0	71.4	14.5	1.39	1.56	5.7	5.0
p4	35	1.01	0.53	13.3	52.5	34.2	15.0	51.6	33.4	1.50	1.53	6.6	2.5
p5	5	1.38	0.78	9.5	65.2	25.3	10.6	58.9	30.6	1.56	1.65	21.2	27.6
p6	120	1.07	0.43	15.5	67.9	16.6	20.1	66.4	13.6	1.43	1.57	8.4	2.7
p7	120	1.05	0.46	13.6	70.9	15.5	19.1	66.9	14.0	1.53	1.54	8.8	6.2
p8	20	1.02	0.44	13.7	71.0	15.3	18.0	67.4	14.7	1.59	1.55	5.5	5.8
p9	50	1.26	0.34	17.0	74.0	9.1	21.3	66.3	12.5	1.45	1.54	5.9	2.8
p10	45	1.10	0.38	11.5	62.1	26.4	16.8	54.8	28.4	1.44	1.58	5.5	4.8
p11	70	0.98	0.40	13.5	70.8	15.7	16.9	61.7	21.4	1.58	1.51	2.7	1.3
p12	70	1.06	0.60	14.1	70.1	15.8	15.9	69.7	14.4	1.54	1.61	4.1	3.1
p13	45	1.14	0.55	10.9	74.3	14.8	15.2	59.6	25.2	1.46	1.71	6.8	23.1
p14	35	1.11	0.36	10.7	74.1	15.3	14.6	56.7	28.7	1.61	1.64	5.6	8.7
p15	60	1.09	0.39	15.5	67.9	16.7	16.8	65.1	18.1	1.36	1.62	6.2	2.7
p16	0	1.07	-	11.3	63.5	25.2	-	-	-	1.54	1.67	11.5	59.6
p17	20	1.19	0.31	12.5	55.6	31.9	15.1	37.5	47.4	1.62	1.67	7.8	36.9
p18	20	1.10	0.49	17.9	58.2	23.9	14.8	52.9	32.2	1.42	1.62	7.2	5.2

Table S3 Estimated soil hydraulic properties, water content at saturation θ_s, residual water content θ_r, inverse of the air entry pressure α, slope parameter n and saturated hydraulic conductivity K_s according to Mualem/Van Genuchten for the two layers Ap1 and Ap2 of the plough horizon and the B horizon

	Ap1					Ap2					B				
	θ_s cm^3 cm^{-3}	θ_r cm^3 cm^{-3}	α cm^{-1}	n -	K_s cm h^{-1}	θ_s cm^3 cm^{-3}	θ_r cm^3 cm^{-3}	α cm^{-1}	n -	K_s cm h^{-1}	θ_s cm^3 cm^{-3}	θ_r cm^3 cm^{-3}	α cm^{-1}	n -	K_s cm h^{-1}
p1	0.383	0.082	0.0044	1.79	0.114	0.383	0.082	0.0019	1.95	0.261	0.337	0.112	0.0008	2.13	0.007
p2	0.395	0.085	0.0037	2.51	0.166	0.395	0.085	0.0030	2.01	0.223	0.362	0.125	0.0010	2.17	0.006
p3	0.396	0.063	0.0013	1.92	0.029	0.396	0.063	0.0009	1.89	0.082	0.365	0.081	0.0006	2.10	0.030
p4	0.413	0.076	0.0022	1.77	0.022	0.413	0.076	0.0018	1.62	0.161	0.377	0.088	0.0005	1.86	0.001
p5	0.368	0.049	0.0008	2.93	0.025	0.368	0.049	0.0010	2.19	0.257	0.350	0.049	0.0005	6.23	0.017
p6	0.377	0.085	0.0028	1.98	0.036	0.377	0.085	0.0013	3.34	0.312	0.371	0.112	0.0009	2.31	0.010
p7	0.477	0.076	0.0017	2.11	0.083	0.477	0.076	0.0011	2.35	0.315	0.356	0.104	0.0006	2.33	0.008
p8	0.370	0.079	0.0013	2.38	0.011	0.370	0.079	0.0012	2.30	0.095	0.370	0.099	0.0008	2.65	0.003
p9	0.394	0.094	0.0012	2.79	0.008	0.394	0.094	0.0008	3.08	0.053	0.355	0.118	0.0009	2.23	0.021
p10	0.378	0.069	0.0047	1.49	0.103	0.378	0.069	0.0019	1.60	0.116	0.369	0.094	0.0011	1.57	0.012
p11	0.381	0.080	0.0026	1.57	0.032	0.381	0.080	0.0019	1.61	0.092	0.375	0.098	0.0014	1.56	0.021
p12	0.351	0.082	0.0035	1.97	0.016	0.351	0.082	0.0045	1.63	0.065	0.359	0.092	0.0015	1.78	0.008
p13	0.370	0.065	0.0008	2.18	0.012	0.370	0.065	0.0005	2.25	0.105	0.328	0.070	0.0010	2.01	0.034
p14	0.420	0.065	0.0010	2.34	0.019	0.420	0.065	0.0007	2.20	0.112	0.383	0.080	0.0006	2.27	0.031
p15	0.399	0.087	0.0015	2.12	0.013	0.399	0.087	0.0016	1.76	0.221	0.391	0.096	0.0010	1.61	0.014
p16	0.405	0.063	0.0017	2.23	0.051	0.405	0.063	0.0015	2.39	0.132	0.358	0.028	0.0014	3.63	0.027
p17	0.401	0.072	0.0015	2.27	0.034	0.401	0.072	0.0010	2.73	0.235	0.319	0.057	0.0011	2.99	0.041
p18	0.403	0.097	0.0004	2.92	0.007	0.403	0.097	0.0003	2.08	0.714	0.401	0.085	0.0002	1.43	0.008

Table S4 Mean absolute error MAE, root mean square error RMSE, model efficiency ME, coefficient of determination R^2 between measurement and AgroC model result for sites p1 to p18 on soil temperature T (subscripts refer to measurement depth in cm) and soil water content θ (subscripts refer to measurement depth in cm)

	T_{10}	T_{20}	T_{50}	θ_{10}	θ_{20}	θ_{50}	T_{10}	T_{20}	T_{50}	θ_{10}	θ_{20}	θ_{50}
	°C	°C	°C	cm^3 cm^{-3}	cm^3 cm^{-3}	cm^3 cm^{-3}	°C	°C	°C	cm^3 cm^{-3}	cm^3 cm^{-3}	cm^3 cm^{-3}
			P3						P1			
MAE	1.20	0.79	1.56	0.012	0.010	0.012	1.34	0.90	1.32	0.013	0.019	0.019
RMSE	1.58	0.96	1.76	0.016	0.013	0.015	1.66	1.08	1.53	0.017	0.024	0.024
ME	0.85	0.90	0.38	0.93	0.97	0.96	0.84	0.88	0.58	0.92	0.90	0.92
R^2	0.87	0.93	0.92	0.93	0.97	0.96	0.87	0.90	0.89	0.92	0.91	0.93
			P5						P4			
MAE	2.30	1.11	1.01	0.014	0.010	0.008	1.46	0.96	1.52	0.015	0.017	0.014
RMSE	3.15	1.44	1.25	0.019	0.014	0.010	1.79	1.17	1.76	0.019	0.023	0.019
ME	0.64	0.82	0.80	0.90	0.94	0.96	0.81	0.85	0.39	0.93	0.91	0.93
R^2	0.73	0.85	0.84	0.91	0.94	0.99	0.83	0.90	0.91	0.93	0.91	0.93
			P7						P6			
MAE	1.33	0.80	1.06	0.015	0.020	0.017	1.81	0.87	1.15	0.018	0.014	0.013
RMSE	1.74	0.99	1.31	0.017	0.026	0.020	2.26	1.09	1.43	0.021	0.017	0.017
ME	0.84	0.90	0.70	0.91	0.87	0.89	0.76	0.88	0.65	0.85	0.93	0.94
R^2	0.87	0.91	0.84	0.93	0.88	0.92	0.78	0.88	0.77	0.89	0.94	0.95
			P8						P10			
MAE	1.19	0.74	1.30	0.015	0.014	0.015	2.17	0.87	1.34	0.010	0.017	0.014
RMSE	1.49	0.92	1.56	0.020	0.018	0.021	2.74	1.05	1.57	0.013	0.023	0.018
ME	0.87	0.90	0.60	0.93	0.95	0.93	0.70	0.86	0.54	0.96	0.91	0.93
R^2	0.89	0.94	0.89	0.93	0.96	0.93	0.74	0.94	0.90	0.96	0.92	0.93
			P9						P11			
MAE	1.38	0.77	1.15	0.022	0.021	0.020	1.78	1.00	1.42	0.010	0.012	0.010
RMSE	1.80	0.93	1.36	0.026	0.025	0.023	2.27	1.24	1.69	0.013	0.021	0.013
ME	0.83	0.91	0.68	0.87	0.93	0.90	0.75	0.82	0.49	0.96	0.92	0.97
R^2	0.87	0.92	0.90	0.88	0.94	0.94	0.77	0.89	0.81	0.96	0.92	0.97
			P13						P12			
MAE	2.06	0.81	1.37	0.021	0.015	0.011	1.49	0.83	1.45	0.016	0.020	0.016
RMSE	2.64	1.00	1.61	0.027	0.018	0.014	1.84	0.98	1.64	0.019	0.025	0.019
ME	0.72	0.90	0.53	0.84	0.95	0.93	0.81	0.87	0.48	0.93	0.89	0.93
R^2	0.77	0.91	0.89	0.84	0.95	0.93	0.83	0.95	0.87	0.93	0.89	0.93
			P14						P15			
MAE	1.25	0.82	1.34	0.012	0.010	0.011	1.17	0.78	1.30	0.016	0.017	0.014
RMSE	1.55	1.00	1.61	0.015	0.013	0.013	1.45	0.94	1.48	0.020	0.023	0.017
ME	0.86	0.89	0.56	0.94	0.97	0.97	0.86	0.90	0.58	0.91	0.89	0.92
R^2	0.88	0.93	0.88	0.94	0.97	0.97	0.88	0.93	0.96	0.91	0.89	0.92
			P17						P18			
MAE	1.49	0.87	1.25	0.016	0.009	0.004	2.01	0.91	1.29	0.021	0.023	0.017
RMSE	1.95	1.07	1.54	0.020	0.013	0.006	2.56	1.13	1.55	0.028	0.032	0.023
ME	0.81	0.89	0.62	0.88	0.97	0.98	0.72	0.88	0.60	0.75	0.81	0.91
R^2	0.84	0.90	0.86	0.88	0.97	0.98	0.75	0.89	0.90	0.78	0.83	0.93

Table S5 Main basic sugar beet growth parameters

parameter value	unit	parameter	description
-20, -50, -4000, -16000	cm	h_0, h_1, h_2, h_3	water stress threshold pressure heads
2.0	°C	T_{base}	base temperature juvenile leaf area growth
0.0015	ha leaf kg^{-1} DM	S_{la}	specific leaf area of new leaves
45.0	kg CO_2 ha^{-1} leaf h^{-1}	A_{mx}	potential CO_2-assimilation rate
0.5	(kg CO_2 ha^{-1} leaf h^{-1}) (J m^{-2} s^{-1})$^{-1}$	E_{ff}	initial light use efficiency
0.69	-	R_{kdf}	extinction coefficient diffuse PAR
3.75	ha ha^{-1}	R_{LAIcr}	critical LAI due to self-shading

Table S6 Relative root depth against relative root density

relative root depth [-]	root density [-]
0.09	1.31
0.30	1.38
0.51	1.01
0.69	0.78
0.90	0.69
1.00	0.61

Fig. S7 Measured soil temperature at sampling location p2 and AgroC simulation

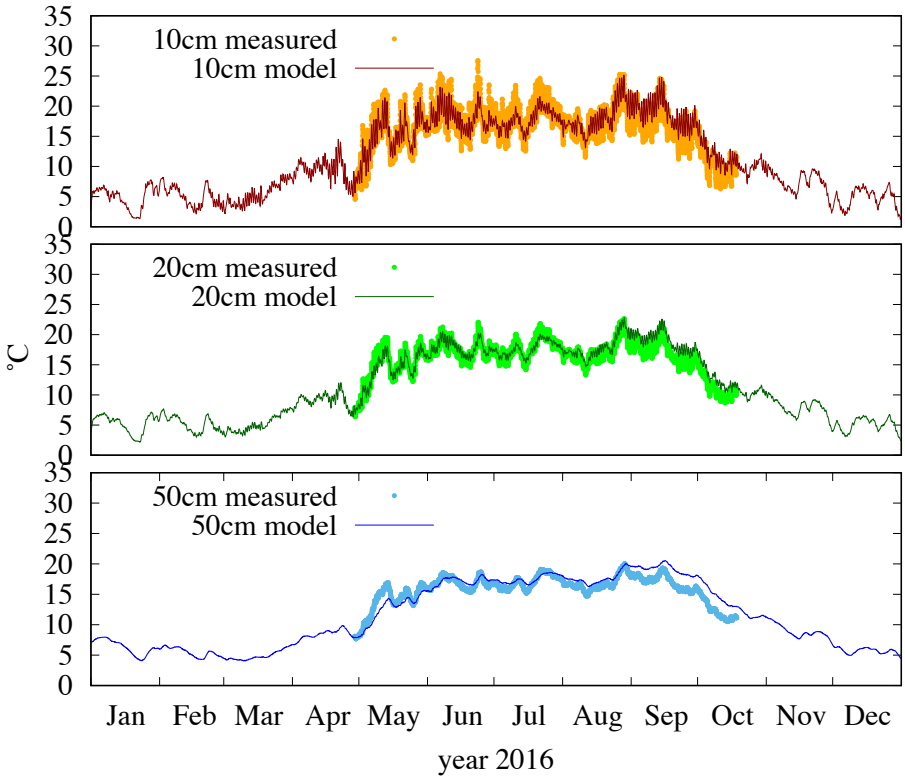

Fig. S8 Measured soil temperature at sampling location p16 and AgroC simulation

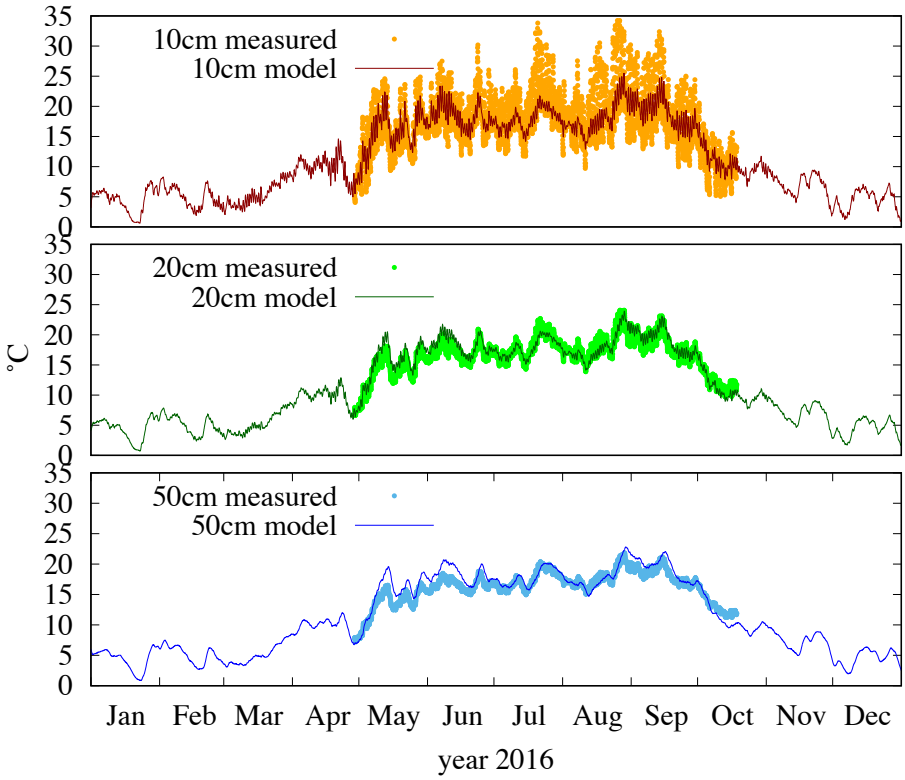

Fig. S9 Observation period average footprint weight and spatial distribution of the loamy cluster (= inside paleo-channel area)